

Article

Genetic Relationship between Mississippi Valley-Type Pb–Zn Mineralization and Hydrocarbon Accumulation in the Wusihe Deposits, Southwestern Margin of the Sichuan Basin, China

Guozhi Wang ^{1,2,*}, Qing Lei ² , Zhu Huang ², Gang Liu ², Yuzhen Fu ², Na Li ² and Jinlong Liu ²

¹ State Key Laboratory of Oil and Gas Reservoir Geology and Exploitation, Chengdu University of Technology, Chengdu 610059, China

² Faculty of Earth Sciences, Chengdu University of Technology, Chengdu 610059, China

* Correspondence: wangguozhi66@163.com

Abstract: The coexistence of numerous Mississippi Valley-type (MVT) Pb–Zn deposits and oil/gas reservoirs in the world suggests a close genetic relationship between mineralization and hydrocarbon accumulation. The Wusihe MVT Pb–Zn deposits are located along the southwestern margin of the Sichuan Basin. Based on the spatiotemporal relation between Pb–Zn deposits and paleo-oil/gas reservoirs, ore material sources, and processes of mineralization and hydrocarbon accumulation, a new genetic relationship between mineralization and hydrocarbon accumulation is suggested for these deposits. The Wusihe Pb–Zn deposits are hosted in the Ediacaran Dengying Formation dolostone, accompanied by a large amount of thermally cracked bitumen in the ore bodies. The Pb–Zn deposits and paleo-oil/gas reservoirs are distributed along the paleokarst interface; they overlap spatially, and the ore body occupies the upper part of the paleo-oil/gas reservoirs. Both the Pb–Zn ore and sphalerite are rich in thermally cracked bitumen, in which μm sized galena and sphalerite may be observed, and the contents of lead and zinc in the bitumen are higher than those required for Pb–Zn mineralization. The paleo-oil/gas reservoirs experienced paleo-oil reservoir formation, paleo-gas reservoir generation, and paleo-gas reservoir destruction. The generation time of the paleo-gas reservoirs is similar to the metallogenic time. The source rocks from the Cambrian Qiongzhusi Formation not only provided oil sources for paleo-oil reservoirs but also provided ore-forming metal elements for mineralization. Liquid oil with abundant ore-forming metals accumulated to form paleo-oil reservoirs with mature organic matter in source rocks. As paleo-oil reservoirs were buried, the oil underwent in situ thermal cracking to form overpressure paleo-gas reservoirs and a large amount of bitumen. Along with the thermal cracking of the oil, the metal elements decoupled from organic matter and H_2S formed by thermochemical sulfate reduction (TSR) and minor decomposition of the organic matter dissolved in oilfield brine to form the ore fluid. The large-scale Pb–Zn mineralization is mainly related to the destruction of the overpressured paleo-gas reservoir; the sudden pressure relief caused the ore fluid around the gas–water interface to migrate upward into the paleo-gas reservoirs and induced extensive metal sulfide precipitation in the ore fluid, resulting in special spatiotemporal associated or paragenetic relations of galena, sphalerite, and bitumen.

Keywords: MVT Pb–Zn deposit; bitumen; ore-forming material source; mineralization; hydrocarbon accumulation



Citation: Wang, G.; Lei, Q.; Huang, Z.; Liu, G.; Fu, Y.; Li, N.; Liu, J. Genetic Relationship between Mississippi Valley-Type Pb–Zn Mineralization and Hydrocarbon Accumulation in the Wusihe Deposits, Southwestern Margin of the Sichuan Basin, China. *Minerals* **2022**, *12*, 1447. <https://doi.org/10.3390/min12111447>

Academic Editor: Jan Marten Huizenga

Received: 26 September 2022

Accepted: 12 November 2022

Published: 16 November 2022

Publisher's Note: MDPI stays neutral with regard to jurisdictional claims in published maps and institutional affiliations.



Copyright: © 2022 by the authors. Licensee MDPI, Basel, Switzerland. This article is an open access article distributed under the terms and conditions of the Creative Commons Attribution (CC BY) license (<https://creativecommons.org/licenses/by/4.0/>).

1. Introduction

Mississippi Valley-type (MVT) zinc–lead (Zn–Pb) deposits are carbonate-hosted epigenetic stratabound deposits and are believed to form from basinal brines [1]. Numerous MVT Pb–Zn deposits show special spatiotemporal associated or paragenetic relationships and genetic links with paleo-oil reservoirs [1–8]. Bitumen, as a common byproduct of hydrocarbon formation, is direct evidence of the existence of oil/gas reservoirs in these deposits. Abundant bitumen has been found in many MVT Pb–Zn deposits, such as the famous

Mississippi Valley [9], Nova Scotia [1], Nanisivik [10], Canada Pine Point ore field [11], Canada Nunavut Polaris [12], Ireland and Scotland [13], China Jinding [14]. The close relationship between Pb–Zn deposits and crude oil, natural gas, and other hydrocarbons are considered to be enigmatic [3].

Many studies have suggested that the ore fluids of Pb–Zn deposits and the hydrocarbon fluids in paleo-oil reservoirs formed via different sources. Among them, the ore fluid is from oilfield brine [15], in which the metal exists in the form of a chloride complex [16]. Hydrogen sulfide required for mineralization is mainly supplied through bacterial sulfate reduction (BSR) or thermochemical sulfate reduction (TSR) [1,3,5,6,8,14,16,17]. When the ore fluids are transported into the oil reservoirs, metals in the ore fluid incorporate with H₂S in the oil reservoirs to form Pb–Zn deposits and result in the coexistence of MVT Pb–Zn deposits and bitumen [1,5,9,17–19]. Many MVT Pb–Zn deposits are explained by this genetic model.

In fact, some low-temperature hydrothermal metal deposits coexist with paleo-oil reservoirs in many sedimentary basins, especially in basins with Au, As, Hg, Sb, and Tl deposits [20,21]. The ore fluids of hydrothermal metal deposits and the hydrocarbon fluids in paleo-oil reservoirs originated from the same sources, and both originated from the source rocks forming the oil reservoirs [1,20,21]. The organic liquids may be relatively rich in metals and may act as transporting agents for ore components [22]. The ore fluid and oil share the same sources, as well as similar co-transportation and co-accumulation processes [20,21,23,24]. The analysis of Pb and Zn contents in crude oil and oilfield brine shows that oil can serve as transporting agents of lead and zinc or forms part of ore fluid [9,22,25–28]. Therefore, the oil and metal–organic complexes in oil are transported and accumulate together, and the destruction of oil reservoirs or gas reservoirs results in mineralization. Mineralization in certain MVT Pb–Zn deposits have been attributed to this genetic model [7,8,27,28].

Abundant bitumen has been found in the Wusihe MVT Pb–Zn deposit located in the southwestern margin of the Sichuan Basin, an ideal place to study the genetic relationship between mineralization and hydrocarbon accumulation. These Pb–Zn deposits mainly occur in dolomites of the Ediacaran Dengying Formation. Up to now, the relationship among mineralization, paleo-oil reservoir formation, and paleo-gas reservoir formation for the Wusihe Pb–Zn deposits is still not completely clear. Studies on ore fluids [29,30], metallogenic periods [31], ore material sources [32–35], and metallogenic mechanisms [29,33] have been performed ever since they were discovered. The ore fluids and hydrocarbon fluids originated from different sources; the metal-rich ore fluids migrated into the oil reservoir, where they combined with hydrogen sulfide formed by the processes of TSR and BSR, resulting in Pb–Zn mineralization; this traditional metallogenic model was suggested for the Wusihe MVT Pb–Zn deposits [29,32,33]. However, our research on these deposits found that the ore fluids and the hydrocarbon fluids in paleo-oil reservoirs were from the same source rocks and that Pb–Zn mineralization was closely related to the destruction of the paleo-gas reservoirs. Therefore, in this paper, based on the spatiotemporal relation of Pb–Zn deposits and paleo-oil reservoirs/paleo-gas reservoirs, ore material sources, and processes of mineralization and hydrocarbon accumulation or destruction, a new genetic relationship between mineralization and hydrocarbon accumulation is suggested for the MVT Pb–Zn deposits.

2. Geological Setting

The Wusihe area is located in the southwestern margin of the Sichuan Basin, which is in the northern margin of the Sichuan–Yunnan–Guizhou (SYG) metallogenic province; the north side is connected to the Dabashan orogenic belt and the southwest side is adjacent to the Longmenshan orogenic belt (Figure 1a). The Sichuan–Yunnan–Guizhou (SYG) metallogenic province is an important component of the giant South China low-temperature metallogenic domain [36]. More than 400 carbonate-hosted Pb–Zn deposits, such as the Wusihe, Chipu, Maozu, Daliangzi, Xichang, Jinshacheng, Lehong, Maliping, and Huize

Pb–Zn deposits (the location in Figure 1a), occur in the SYG, yielding total Pb–Zn ores of more than 200 million tons at mean grades of 10 wt.% Zn and 5 wt.% Pb [30]. The study area is mainly composed of basement and Ediacaran to Paleozoic cover sequences. The basement rocks are characterized by a double-layer structure [32,33,36]. The Paleoproterozoic–Paleoproterozoic metamorphic complex constitutes the crystalline basement [36], and the Mesoproterozoic–Neoproterozoic metamorphic fine clastic rocks and carbonate rocks interbedded with metamorphic volcanic sediments constitute the folded basement [37]. The Ediacaran to Paleozoic cover sequences are composed of the early Ediacaran Suxiong Formation, late Ediacaran Guanyinya Formation and Dengying Formation, and the Cambrian–Permian marine sedimentary sequences. The Suxiong Formation is mainly a set of volcanic–sedimentary rocks. The Guanyinya Formation and Dengying Formation are a set of marine sandstone, siliceous and evaporitic carbonate [31,33], respectively. The Cambrian–middle Permian and lower Permian strata mainly consist of carbonate–clastic rock deposits and continental basalt, respectively [31–33]. The Ediacaran Dengying Formation is not only the main host of MVT Pb–Zn deposits [7,8,30,36,38–40] but also an important commercially productive source of natural gas in the Sichuan Basin [41–44]. Many MVT Pb–Zn deposits have been found in the relict paleo-oil/gas reservoirs in the Dengying Formation located in the periphery of the Sichuan Basin [7,8,45]; the Wusihe Pb–Zn deposits located in the southwestern margin of the Sichuan Basin is one representative example of these deposits. The gas reservoirs in the Dengying Formation, such as the Gaoshiti and Moxi gas reservoirs, are mainly distributed in the deeply buried traps located in the central Sichuan Basin [41–44], and sporadic sphalerite and galena can be observed in these commercially productive natural gas reservoirs.

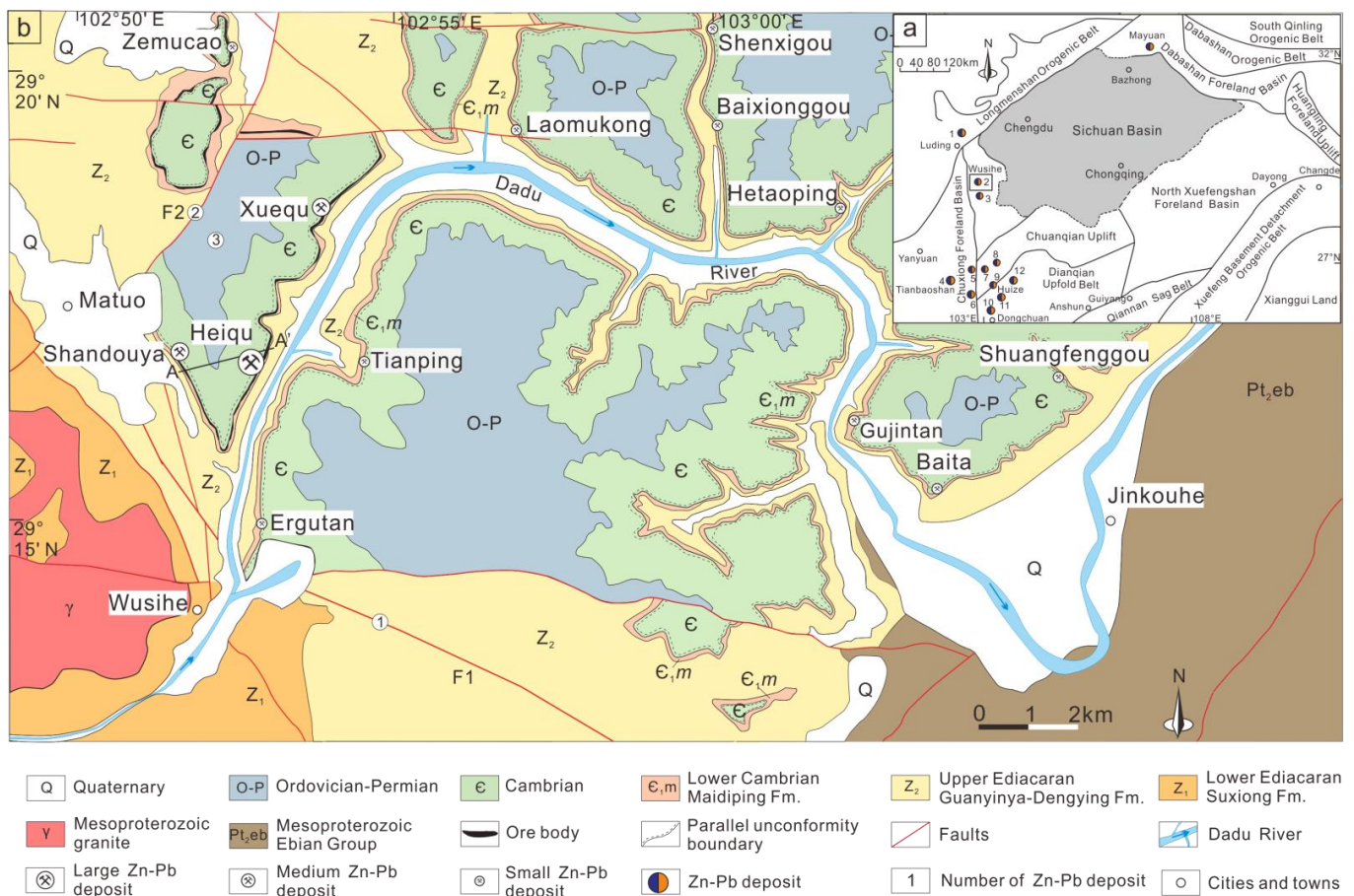


Figure 1. (a) Sketch of the tectonic framework of South China (modified from Li and Zhang, 2012 [32]); (b) Regional geological map of the Wusihe district.

3. Ore Deposit Geology

A more than 50-km-long metallogenic belt is hosted in the Dadu River valley (Figure 1b). Pb–Zn deposits occur within the late Ediacaran–early Cambrian carbonate sequences. Among these Pb–Zn deposits, the Wusihe deposit is the largest and includes the Xuequ, Heiqu, and Shandouya.

3.1. Ore-Bearing Strata

Most ore bodies of the Wusihe deposits are hosted by siliceous dolomite of the Dengying Formation, and a small number of ore bodies are hosted by carbonaceous shale of the lower Cambrian Qiongzusi Formation (Figure 2). The Dengying Formation is in conformable contact with the underlying sandstone of the Guanyinya Formation. According to the lithologic characteristics of the Dengying Formation, it can be divided into five lithologic members from top to bottom (Figure 2). Member I (Z_2d^1) mainly contains gray–dark gray dolomicrite and microcrystalline dolostone that are partially intercalated with clastic rock, and this member is 160.1 m thick. Member II (Z_2d^2) is mainly composed of gray–light gray microcrystalline–crystalline powder dolostone, algal mass dolostone, botryoidal dolostone, forming rhythmic interbedding, and occasional breccia dolostone, and this member is 406.7 m thick; the dolostone in this member is characterized by a botryoidal structure, dissolved pores, and karst caves. Member III (Z_2d^3) mainly contains light gray–dark gray laminated dolomicrite and microcrystalline dolostone, algal laminated dolostone interbedded with multilayer yellow–gray clayey dolostone–dolomitic mudstone. The thickness of this member is 81.0 m. Member IV (Z_2d^4) is mainly gray–white dolomicrite and microcrystalline dolostone, pinhole dolostone, and laminated dolostone, and it is 155.1 m thick. The Maidiping Member is mainly composed of dolomicrite and banded siliceous rocks, which are interbedded and have unequal thicknesses. Karst breccia approximately one meter thick can be observed at its top; this member is 176 m thick. Among them, Member I–Member IV are late Ediacaran in age, and the Maidiping Member is part of the early Cambrian strata. Two paleokarst interfaces have been identified between the Qiongzhusi Formation and the Maidiping Member, the Member III and the Member II, respectively. The MVT Pb–Zn deposits and paleo-oil/gas reservoirs are mainly distributed along the paleokarst interfaces, and sphalerite, galena, and bitumen mainly fill dissolved pores and cavities (Figure 2). The Pb–Zn deposits occurring at the paleokarst interface between the Member III and the Member II, the Qiongzhusi Formation and the Maidiping Member are represented by the Tuanbaoshan Pb–Zn deposit and Wusihe Pb–Zn deposit, respectively, in which the ore bodies are stratiform-like. The Qiongzhusi Formation is mainly composed of dark gray mud shale and siltstone, and a small number of veined and stratiform-like ore bodies may be observed in the Qiongzhusi Formation. Bitumen with different abundances can be identified in these ore bodies.

3.2. Spatial Relationship between Paleo-Oil/Gas Reservoirs and Pb–Zn Deposit

Field geological surveys and laboratory research showed that abundant massive, spherical, hemispherical, and irregular bitumen filled in dissolved pores, cavities, and fractures in the Dengying Formation and is distributed along the paleokarst interface. Bitumen is a common byproduct within matured or over-matured oil/gas reservoirs. The bitumen in the Dengying Formation is pyrobitumen [41,44–47], and it formed during in situ transformation from paleo-oil reservoirs to paleo-gas reservoirs; therefore, the location of the bitumen retained today is equivalent to the location of the paleo-oil/gas reservoirs. According to the abundance and distribution of bitumen in dissolved pores and karst cavities, two relict paleo-oil/gas reservoirs are preserved along the paleokarst interface (Figure 2). The shale of the Qiongzhusi Formation is the regional cap rock of paleo-oil/gas reservoirs in the Maidiping Member. The Wusihe Pb–Zn deposits mainly occur in paleo-oil/gas reservoirs in the Maidiping Member, and a small amount is present in the Qiongzhusi Formation. The roof of the ore bodies is the shale of the Qiongzhusi Formation, and the floor of the ore bodies is bituminous dolostone. The ore bodies mainly occupy the

upper part of the paleo-oil/gas reservoirs, and a small number of them developed in the cap rocks close to the paleo-oil/gas reservoirs (Figure 2).

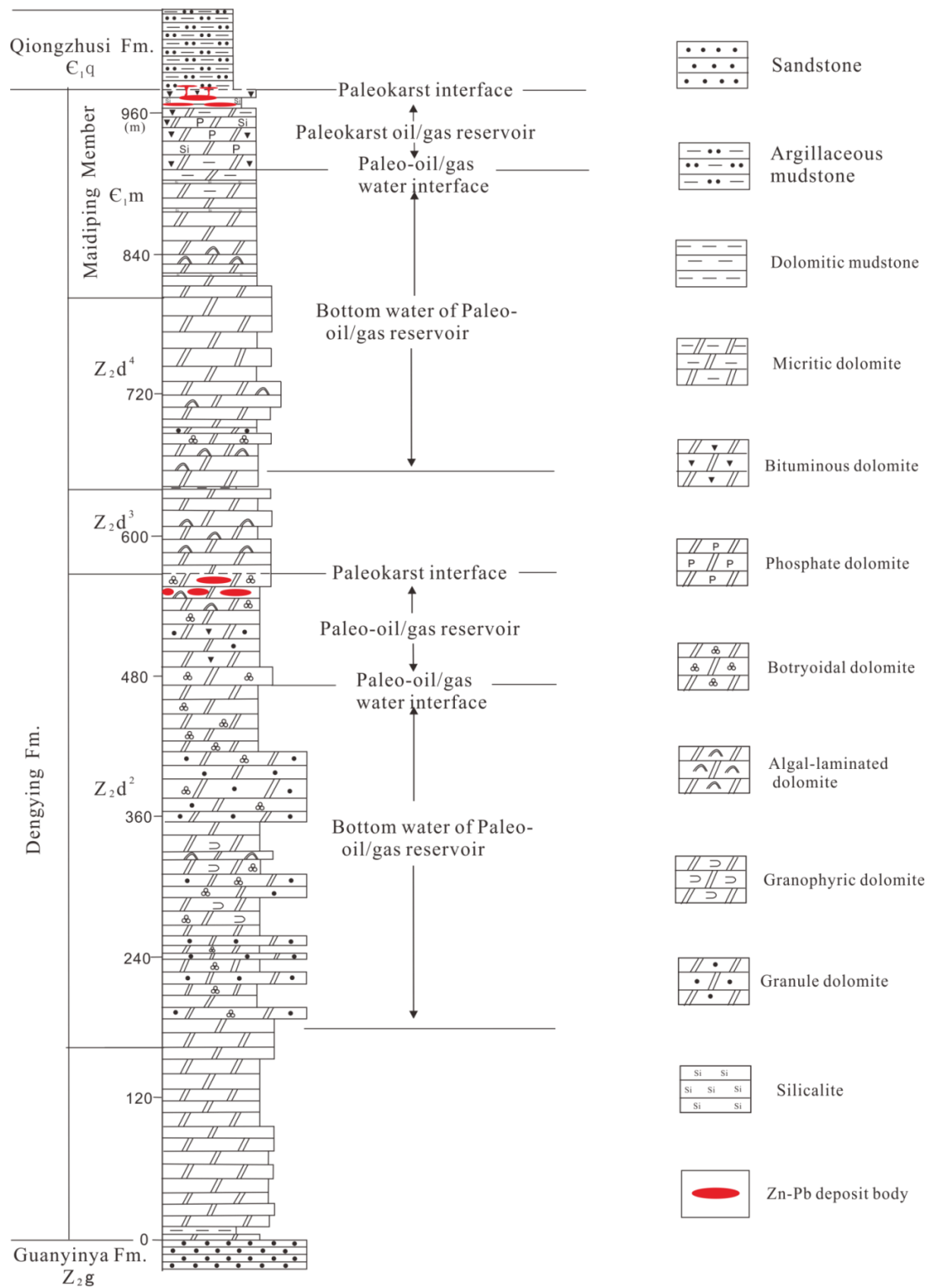


Figure 2. Lithological column and distribution of Zn–Pb deposits and oil/gas reservoirs.

3.3. Ore Bodies

Geological investigations demonstrated that the Wusihe deposits are mainly exposed in the Xuequ-Shandouya syncline within an area about 3.7 km long and 2.5 km wide

(Figure 1b). The syncline strike nearly towards the N-S direction, and its eastern limb dips 5–16° while the western limb dips 5–22°. They are hosted by the carbonaceous shale of the Lower Cambrian Qiongzusi Formation and the siliceous dolomite of the Maidiping Member (Figure 3). The ore bodies in the Maidiping Member predominantly exhibit stratabound and lenticular in shape and parallel to the bedding of the host rocks. The ore bodies in the Qiongzhusi Formation are mainly in the form of steeply dipping veins, and they are connected downward with the stratiform ore bodies in the Maidiping Member; sometimes, they extend laterally for several meters to tens of meters along the bedding on both sides of a vein before naturally pinching out (Figure 3a). Ore bodies have variable thicknesses ranging from 0.20–2.97 m, with a mean of 0.93 m [33]. Sphalerite and galena in the Maidiping Member are mainly filled in the dissolved pores and cavities in silicified dolostones and siliceous rocks. Sphalerite and galena in the Qiongzhusi Formation are filled in the fractures or stratiform pore spaces (Figure 3a).

The ores are dominantly sulfides with a relatively simple mineral association, in which sphalerite is the most abundant economic mineral (Figure 3b); in contrast, galena, pyrite, and chalcopyrite are minor. Sphalerite and galena can either coexist or occur independently. Gangue minerals are primarily bitumen, quartz, dolomite, calcite, and occasional barite. The bitumen (Figure 3c–g) is abundant in the ore. The ores often have massive (Figure 3b), banded and disseminated structures and occasional spherical structures. Bitumen, galena, and sphalerite mainly occupy different pores and cavities (Figure 3d) or the same pores and cavities distributed along the paleokarst interface (Figure 3e–g). Most sphalerites are yellow and yellow-brown spheroids with a concentric banded structure owing to the color and distribution of opaque mineral inclusions (Figure 3d,e,g). Raman spectral analysis of the opaque mineral inclusions in the bands shows that the opaque minerals are mainly bitumen inclusions (Figure 3g,h). Quartz and dolomite show an obvious two-generation relationship. Quartz and dolomite in the early stage are mostly distributed at the edges of the dissolved pores, while quartz (Q_2) and dolomite (Dol_2) in the late stage are often filled in the centers of the same dissolved pores with bitumen (Bit_2) and sphalerite (Sp_2), showing an obvious paragenetic relationship (Figure 3e–g).

Previous analyses show that the ore bodies and paleo-oil/gas reservoirs overlap spatially, and the ore bodies mainly occupy the upper part of the paleo-oil/gas reservoirs. Abundant bitumen is paragenetic with sphalerite and galena in the ores, and there are bitumen inclusions in the sphalerite, which show a close coexisting spatial relationship between the paleo-oil/gas reservoirs and the Pb–Zn deposits.

3.4. Stages of Mineralization

The above discussion shows that the bitumen is pyrobitumen, and most of the bitumen was formed during the transformation from the paleo-oil reservoir to the paleo-gas reservoir; therefore, pyrobitumen can be used as a time constraint, and other minerals can be placed on the same time axis to determine their relative temporal relationship.

According to petrographic observations, the bitumen in the study area can be divided into early and late stages. The bitumen in the early stage (Bit_1) is mainly distributed at the edge of the pores and attached to the inner side of the hole in a ring shape (Figure 3f), while the bitumen in the late stage (Bit_2) is distributed in the center of the pores and often coexists with euhedral conical quartz or euhedral–subhedral dolomite (Figure 3e–g). The early bitumen (Bit_1) was mainly formed during the transformation from the paleo-oil reservoir to the paleo-gas reservoir, and the late bitumen (Bit_2) was formed during the adjustment or destruction process of the paleo-gas reservoir; it was the reprecipitation product of the early bitumen (Bit_1) in the water at the bottom of the oilfield. According to the relative temporal relationship between the minerals and bitumen filling different pores, mineralization can be divided into early and late stages, forming two different generations of minerals (Figure 4).

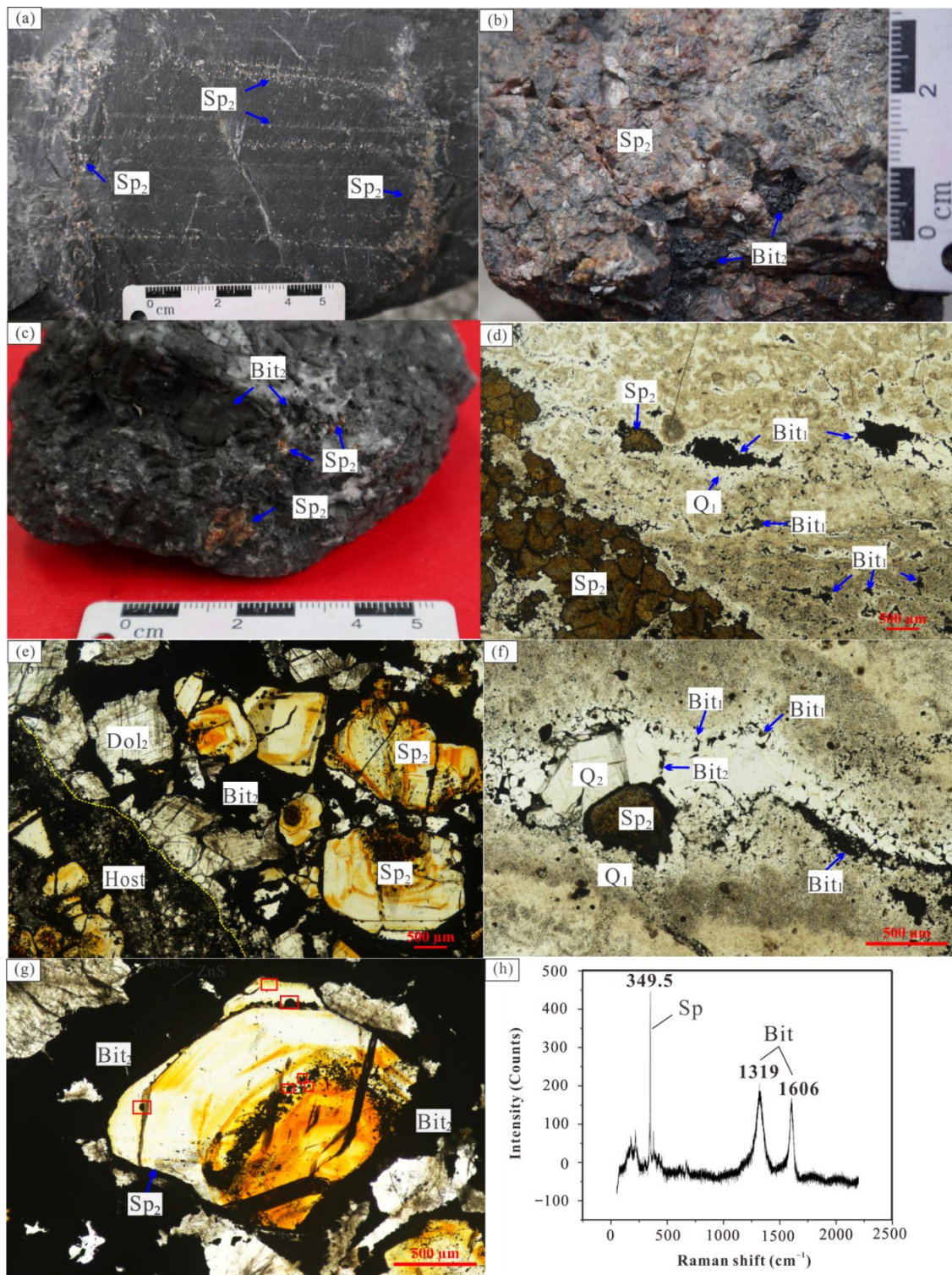


Figure 3. Spatiotemporal relationship between sphalerite and bitumen in ores. (a) The sphalerite (Sp₂) in the Qiongzhusi Formation is veined and stratiform; (b) Massive structure shown bitumen (Bit₂) in sphalerite (Sp₂), and the host stratum is the Maidiping Member; (c) Sphalerite (Sp₂) shown in bituminous dolostone, and the host stratum is the Maidiping Member; (d) Quartz, bitumen and sphalerite fill in the pore space and fractures, and the host rocks are the silicified dolostone in the Maidiping Member; sphalerite and bitumen are filled in different pore space, showing the filling sequence: quartz (Q₁) → bitumen (Bit₁) → sphalerite (Sp₂); (e) Sphalerite (Sp₂), bitumen (Bit₂) and dolomite (Dol₂) are filled in the same pore space in dolostone in the Maidiping Member; (f) Sphalerite

(Sp₂), bitumen (Bit₁, Bit₂) and quartz (Q₁, Q₂) are filled in the same pore space in silicified dolostone, showing the filling sequence of quartz (Q₁) → bitumen (Bit₁) → sphalerite (Sp₂) + quartz (Q₂) + bitumen (Bit₂); (g) Banded sphalerite (Sp₂) is paragenetic with bitumen (Bit₂), and the red box in the figure shows the Raman spectroscopic analysis of inclusions; (h) Raman analysis of inclusions in sphalerite (Sp₂) shows that the inclusions are bitumen, as shown in the red box in (g). Sp sphalerite, Q quartz, Bit bitumen, Dol dolomite, Host rock.

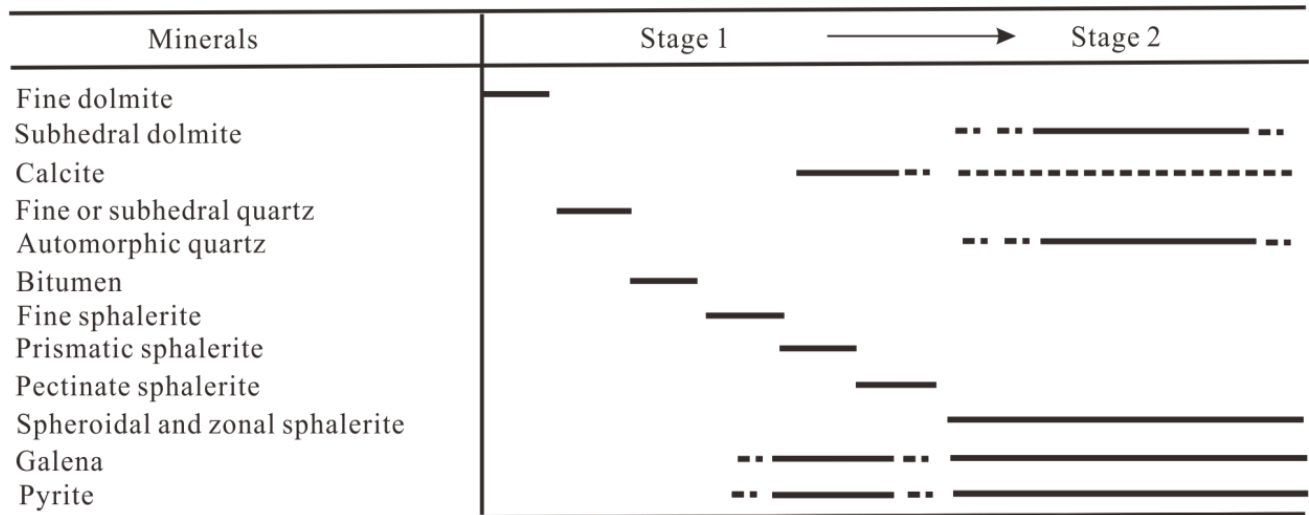


Figure 4. Schematic summary of mineral paragenesis in the Wusihe deposit.

The sphalerite that formed in the early stage of mineralization is characterized by fine grains, dentate and comb shapes, and limited inclusions. In some cavities, fine-grained sphalerite aggregates (Sp₁¹), dentate sphalerite (Sp₁²), and comb-shaped sphalerite (Sp₁³) are filled in turn from the edge to the center of the cavities (Figure 5a). The sphalerite (Sp₂) formed in the late stage is mostly spherical, with particles ranging from 3 mm–2 cm, most of them having a concentric banded structure (Figures 3e,g and 5f), and some bitumen and few host rocks are encapsulated in the sphalerite (Sp₂). Early-formed minerals, such as fine-grained sphalerite (Sp₁¹) (Figure 5b) and galena (Ga₁) (Figure 5e), and host rocks, such as bituminous dolomite (Figure 5c), pore fillings with bitumen (Bit₁, Bit₂) (Figure 5d) and siltstone (Figure 5c), were encapsulated in late sphalerite (Sp₂), indicating that the late sphalerite (Sp₂) was formed in different periods after the thermally cracked bitumen. Two distinct generations of galena can be identified: early galena is encapsulated in sphalerite (Sp₂) (Figure 5e), and late galena is paragenetic with late sphalerite (Sp₂) (Figure 5f). Sometimes, thermally cracked bitumen inclusions (Bit₁) can be observed in the late galena (Ga₂), indicating that they formed later than thermally cracked bitumen. Two stages of gangue minerals, such as dolomite, calcite, and quartz, can be identified. The early dolomites (Dol₁) are distributed in granular form at the edges of the pores, and the bitumen is attached to the early dolomite, forming a ring shape (Figure 5g). The late dolomites (Dol₂) are mostly euhedral–subhedral and closely paragenetic with the late bitumen (Bit₂), sphalerite (Sp₂), and quartz (Q₂) (Figures 3e and 5g). The early quartz (Q₁) is distributed in the edges of pores in fine grain, and the relict pore spaces are filled with bitumen (Figures 3d,f and 5h). The late quartz (Q₂) is mostly euhedral and conical, and it is paragenetic with late bitumen (Bit₂), sphalerite (Sp₂), and dolomites (Dol₂) (Figures 3f and 5g,h). They are characterized by enrichment in single-phase hydrocarbon inclusions [29] and bitumen inclusions (Figure 5h,i). The abundant bitumen inclusions in the late quartz (Q₂) indicate that they formed after the thermally cracked bitumen (Bit₁).

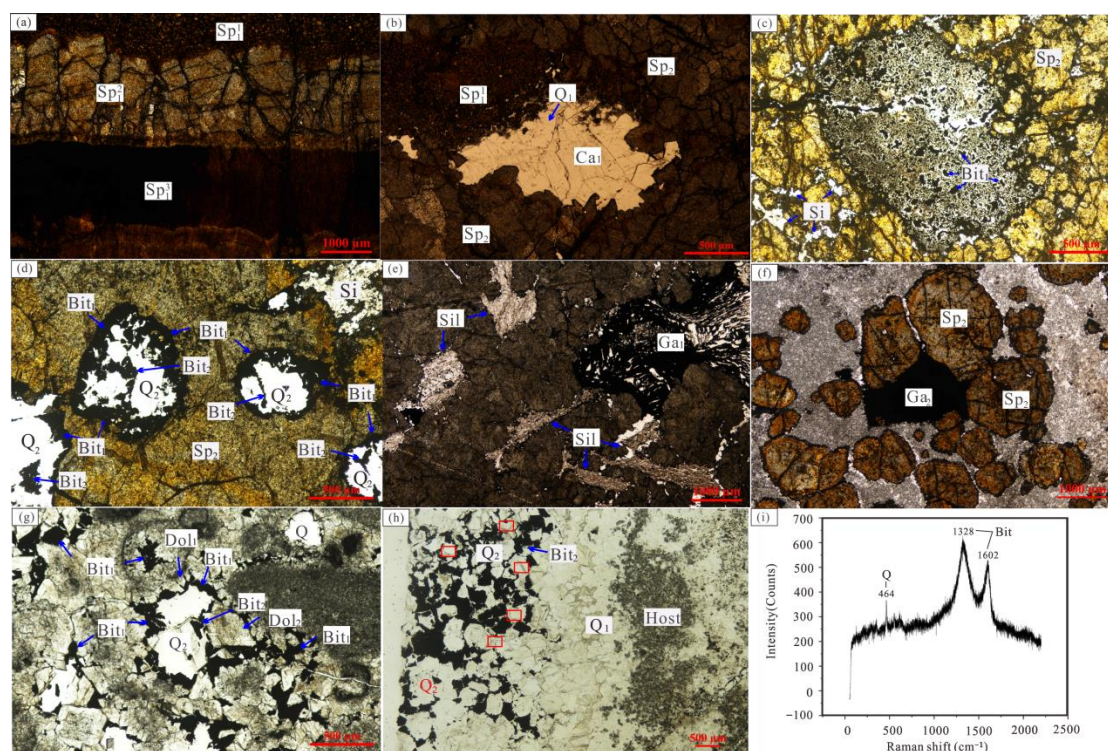


Figure 5. Photomicrographs and Raman spectroscopic analysis of mineral generation relationships. (a) The early spherical spherulite precipitated in a cavities, and the filling order is fine granular spherulite (Sp₁¹) → dentate spherulite (Sp₁²) → comb-shaped spherulite (Sp₁³) from the edge to the center; (b) The early granular spherulite (Sp₁¹), early quartz (Q₁) and calcite (Ca₁) are encapsulated in late spherulite (Sp₂); (c) The host rocks, such as bituminous (Bit₁) silicified dolostone and siliceous rock (Si), are encapsulated in late spherulite (Sp₂); (d) The host rocks, such as pore space fillings and siliceous rock (Si), are encapsulated in late spherulite (Sp₂); among them, two generations of bitumen (Bit₁, Bit₂) can be identified in the pore fillings, suggesting that this spherulite (Sp₂) was formed at the end of the late mineralization; (e) The host rocks, such as siltstone (Sil) and early galena (Ga₁), are encapsulated in late spherulite (Sp₂); (f) Late banded spherulite (Sp₂) is paragenetic with granular galena (Ga₂); (g) The generation relationship of gangue minerals is that the pore was filled with early dolomite (Dol₁) → early bitumen (Bit₁) → late bitumen (Bit₂) + late quartz (Q₂) + late dolomite (Dol₂) from the edge to center of the pore; (h) The generational relationship of gangue minerals is that the pore was filled with early quartz (Q₁) → late bitumen (Bit₂) + late quartz (Q₂) from the edge to center of the pore. The early quartz (Q₁) is xenomorphic granular and has no inclusions. The late quartz is euhedral-subhedral and conical, with abundant banded bitumen inclusions; the red frame shows the position of Raman spectrum analysis of inclusions in late quartz; (i) Raman spectroscopic analysis of bitumen inclusions in late quartz (Q₂). Quartz tested for analysis is marked with red boxes in (h). Sp spherulite, Ga galena, Py pyrite, Q quartz, Bit bitumen, Ca calcite, Dol dolomite, Si siliceous, Sil silty mudstone, Host rock.

4. Samples and Analytical Method

Twelve representative source rock samples in the Qiongzhusi Formation and five bituminous dolomite samples in the Maidiping Member were collected for organic geochemistry analysis. The source rock samples were from the core of the Gaoshi 17 well (GS17-2, GS17-8, GS17-12) and the Moxi 9 well (MX9-1, MX9-2, MX9-3) in the central Sichuan Basin. Bituminous dolomite samples (XQ18-2, XQ18-5, XQ18-8, XQ18-26, and XQ18-33) were from an adit in Xuequ. Organic geochemical analysis of source rocks and bituminous dolomites was performed at the Guangzhou Institute of Geochemistry, Chinese Academy of Sciences. Detailed analytical methods are given in Wu et al. (2008) [48]. The three bitumen samples (XQ18-6, XQ18-10, and XQ18-12) used for scanning electron

microscopy (SEM) analysis were mainly from dolostone at the tops and bottoms of the ore bodies in Xuequ. Bitumen (Bit₁) with slightly larger particles was selected and prepared into thin slices, and the interiors of the bitumen particles were observed by SEM. The source rock samples (ZK601-17, Zk601-18, and Zk601-21) used for SEM analysis were mainly from the core in the Qiongzhusi Formation at Xuequ and prepared into thin slices. SEM analysis was performed at the State Key Laboratory of Oil and Gas Reservoir Geology and Development Engineering, Chengdu University of Technology, Chengdu, China. The selected bitumen samples were analyzed and tested by SEM (model: Nova Nano SEM450) and X-ray energy dispersive spectrometry (EDAX) (model: EDAX AXF-650 Apollo X) under the conditions of 20 kV, 21 °C and 35% relative humidity (RH), based on SY/T5162-1997. The sphalerite (Sp₂) and quartz (Q₂) samples used for Raman spectroscopy analysis were mainly from Pb–Zn ores in Xuequ and Shandouya. The ores were made into thin slices, from which late sphalerite (Sp₂) with a banded structure and late conical quartz (Q₂) with a banded structure were selected for analysis and testing. The Raman spectra of the samples were analyzed by a LabRAM HR Evolution laser confocal microscopy Raman spectrometer produced by HORIBA JOBIN YVON, France, in the Raman Laboratory of the Chengdu University of Technology, with a spectral resolution of 0.65 cm⁻¹. The spectrometer had a focal length of 800 mm, laser wavelength of 532 nm, 50× Leica objective lens, and scanning range of 200–1000 cm⁻¹.

Sixteen representative samples of sulfide ore with different structures, such as massive, laminated, banded, veined, and disseminated, were collected from an adit in Shandouya and Xuequ. The samples were broken into 0.25 to 0.5 mm fragments, handpicked to >95% purity under a binocular microscope, and cleaned ultrasonically. Twenty-seven single sulfides formed in the late stage were selected for bulk sulfur isotope analysis, including sixteen sphalerite and eleven galena samples. Sulfur isotope analyses of sulfide minerals were carried out at the Analysis and Testing Research Center, Beijing Institute of Geology, Nuclear Industry. The samples were crushed to <200 mesh and heated under a vacuum with Cu₂O. The δ³⁴S values of the resulting SO₂ gas were measured on a Delta V plus gas isotope mass spectrometer. The results are reported with an analytical uncertainty of 0.2‰ (2σ). Sulfur isotope compositions are reported relative to Vienna Canyon Diablo Troilite (V-CDT).

5. Results

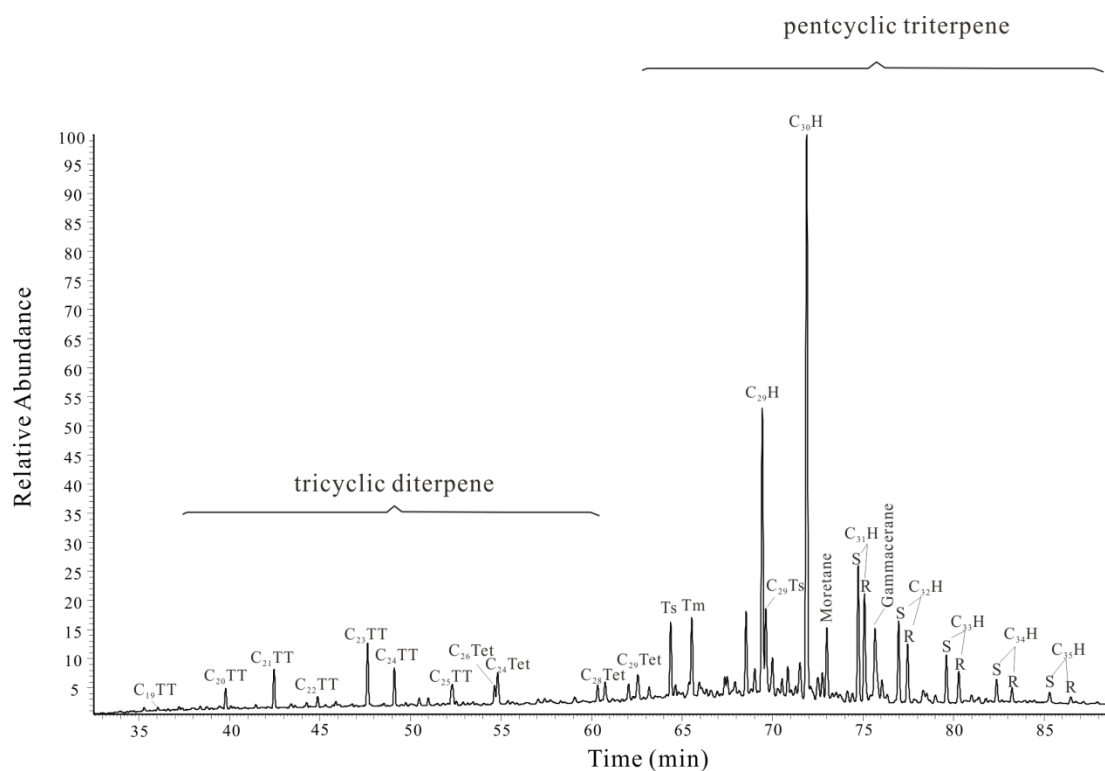
5.1. Characteristics of Biomarkers in Source Rock and Reservoir Bitumen

The biomarkers originate from parental sources of organisms and are preserved in rocks and sediments; there is little or no difference between parental materials and biomarkers in the texture of organic molecules due to their relative stability during diagenesis and secondary alteration [49]. As characteristic organic compounds, biomarkers could provide information about the organic composition of parental materials. The chromatographic parameters of the saturated hydrocarbons in the source rocks from the Qiongzhusi Formation and reservoir bitumen from the Maidiping Member are listed in Table 1. The nC₂₁⁻/nC₂₂⁺, Pr/Ph, Pr/nC₁₇, Ph/nC₁₈, and odd-even predominance (OEP) values of the source rocks are intermediate from 0.63–1.26, 0.47–0.85, 0.49–0.94, 0.53–1.16 and 0.93–1.02, respectively. The nC₂₁⁻/nC₂₂⁺, Pr/Ph, Pr/nC₁₇, Ph/nC₁₈, and OEP values of the reservoir bitumen are intermediate from 0.14–0.58, 0.23–0.95, 0.33–0.50, 0.31–0.43 and 1–1.36, respectively.

The distribution of terpenoid compounds in saturated hydrocarbons from the reservoir bitumen is shown in Figure 6. The C₁₉–C₂₈ series of tricyclic diterpenes and C₂₇–C₃₅ series of pentacyclic triterpanes are dominant. Compared to tricyclic diterpenes, pentacyclic triterpanes are more abundant. They are characterized by C₂₃TT > C₂₁TT > C₂₀TT in tricyclic diterpenes and high gammacerane/αβ-hopane ratios (0.15–0.21) (Table 2). The molecular parameters of terpenes reflecting maturity, such as Ts/(Ts + Tm), C₃₁(22S)/(22S + 22R), and C₃₂(22S)/(22S + 22R), are 0.41–0.51 (average: 0.46), 0.54–0.55 (average: 0.54) and 0.57–0.59 (average: 0.58), respectively (Table 2).

Table 1. The chromatographic parameters of the saturated hydrocarbons in source rocks and reservoir bitumen.

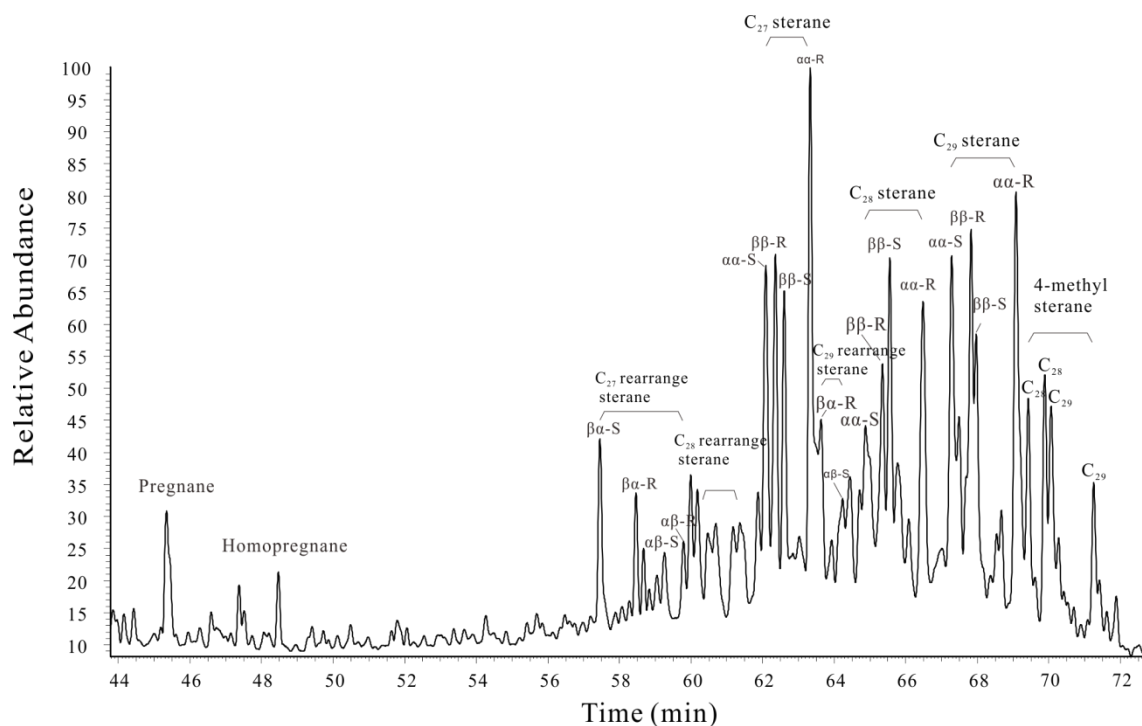
Sample Number	Samples Type	nC_{21}^-/nC_{22}^+	Pr/Ph	Pr/nC ₁₇	Ph/nC ₁₈	OEP
XQ18-2	Bitumen in Maidiping Member	0.40	0.65	0.48	0.32	1.00
XQ18-5		0.58	0.35	0.44	0.43	1.14
XQ18-18		0.18	0.34	0.33	0.37	1.18
XQ18-26		0.14	0.95	0.50	0.31	1.36
XQ18-33		0.21	0.23	0.38	0.35	1.16
MX9-1	Source rocks in Qiongzhusi Fm.	1.14	0.54	0.50	0.53	1.02
MX9-2		1.04	0.47	0.51	0.55	1.01
MX9-3		0.98	0.55	0.49	0.57	1.04
GS17-2		0.63	0.85	0.76	0.71	0.93
GS17-8		1.26	0.67	0.94	1.16	1.01
GS17-12		1.15	0.60	0.60	0.60	1.01

**Figure 6.** The distribution of terpenoid compound in saturated hydrocarbons of organic material from the representative reservoir bitumen in the Maidiping Member (sample number: XQ18-5) (m/z 191 chromatogram-mass spectrum).

The sterane composition of the reservoir bitumen is demonstrated in Figure 7. The sterane is mainly composed of regular sterane, which is characterized by a higher abundance of pregnane and homopregnane and a lower abundance of rearranged sterane. The C₂₉ sterane (0.35–0.38) of the reservoir bitumen is similar to the C₂₇ sterane (0.32–0.36), while the C₂₈ sterane contents are 0.27–0.34 (Table 2). The molecular parameters of sterane reflecting maturity, such as C₂₉ββ/(αα + ββ) and C₂₉αα20S/(20S + 20R), are 0.36–0.43 (average: 0.39) and 0.38–0.45 (average: 0.42), respectively (Table 2).

Table 2. The biomarker parameters of the reservoir bitumen in the Maidiping Member.

Sample Number	XQ18-2	XQ18-5	XQ18-18	XQ18-26	XQ18-33
Ts/Tm	0.84	0.88	0.81	0.69	0.86
Gammacerane/C ₃₀ H	0.17	0.19	0.17	0.16	0.15
Ts/(Ts + Tm)	0.46	0.47	0.45	0.41	0.46
C ₃₁₋₃₅ homohopane/C ₃₀ hopane	0.83	0.92	0.85	0.83	0.79
C ₂₉ Ts/(C ₂₉ Ts + C ₂₉ H)	0.24	0.23	0.24	0.26	0.25
C ₃₁ (22S)/(22S + 22R)	0.54	0.54	0.54	0.54	0.55
C ₃₂ (22S)/(22S + 22R)	0.59	0.57	0.57	0.59	0.59
C ₂₇ regular sterane (%)	0.36	0.34	0.34	0.32	0.34
C ₂₈ regular sterane (%)	0.34	0.29	0.29	0.31	0.31
C ₂₉ regular sterane (%)	0.31	0.37	0.37	0.38	0.35
4-methyl sterane/C ₂₉ Sterane	0.51	0.49	0.55	0.46	0.49
C ₂₉ ββ/(αα + ββ)	0.42	0.43	0.37	0.43	0.38
C ₂₉ αα20S/(αα20S + αα20R)	0.42	0.43	0.41	0.4	0.4

**Figure 7.** The distribution of sterane compounds in saturated hydrocarbons of organic material from representative reservoir bitumen in the Maidiping Member (sample number: XQ18-5) (m/z 217 chromatogram-mass spectrum).

5.2. Metal Minerals in Source Rocks

Based on the analysis of the ore-forming element contents in the source rocks from the Qiongzhusi Formation, representative samples with relatively high lead and zinc contents were selected for SEM analysis. Microsized galena, sphalerite, siderite, barite, and pyrite were found in the source rocks from the Qiongzhusi Formation at Xuequ (Figure 8). The galena is irregularly rectangular in shape; they are 1.1 μm \times 1.4 μm –10.6 μm \times 16.9 μm in size. The sphalerite is rhombus in shape or occurs as inclusion encased in cubic pyrite; rhombus sphalerite is 30.9 μm \times 32.3 μm in size. There are two forms of pyrite: cubic crystals (4.5 μm \times 7.5 μm –34.3 μm \times 41.1 μm) and mildew spheres (6 μm –9 μm). The barite is round in shape and 2.2 μm \times 3.6 μm in size.

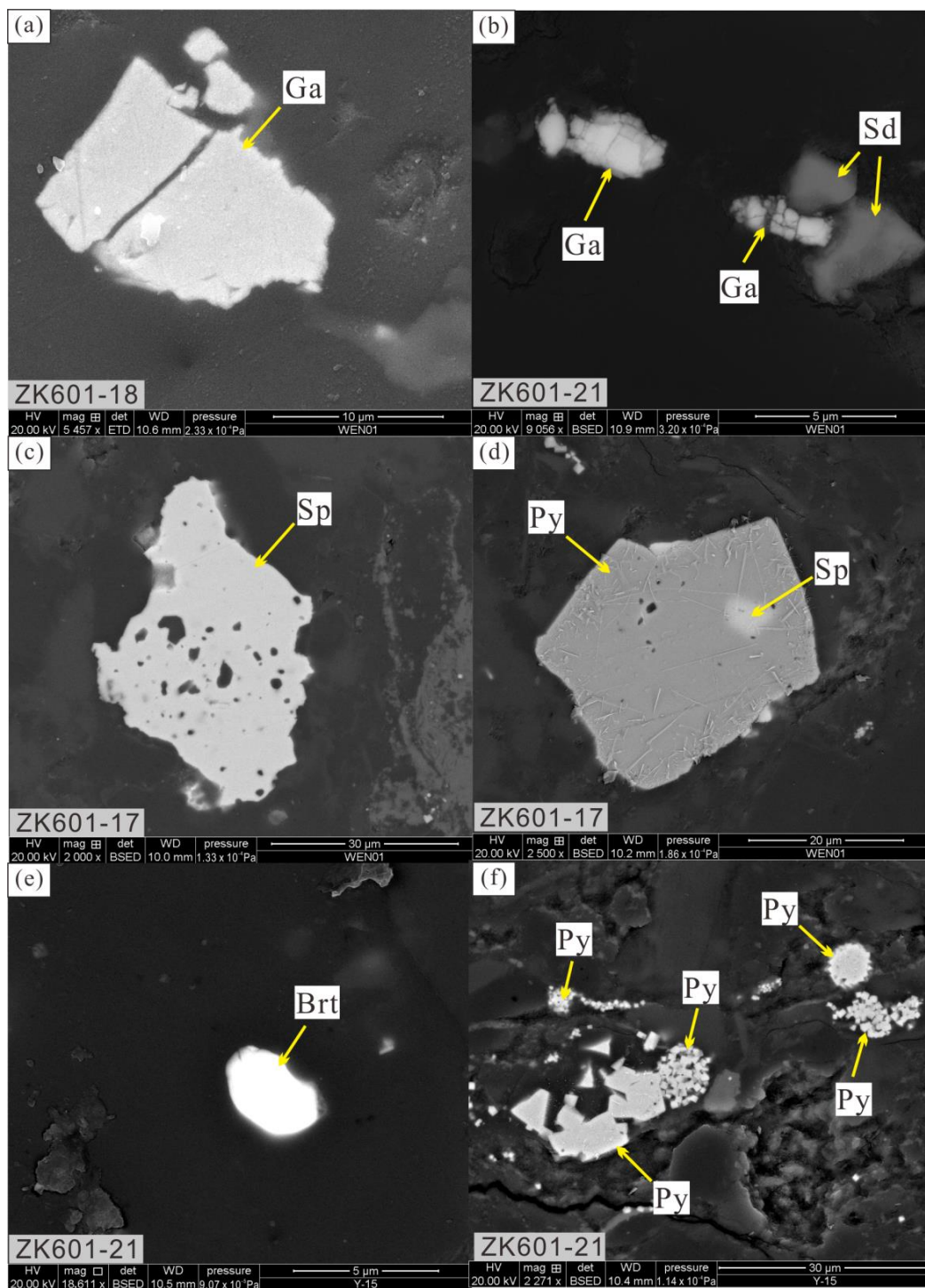


Figure 8. SEM observation results of source rocks at Xuequ (sample Nos.: ZK601-17, ZK601-18 and ZK601-21). (a) A galena in the source rocks; (b) Some galenas and siderite in the source rocks; (c) Asphalerite in the source rocks; (d) A pyrite in the source rocks, sphalerite is encased in the interior of the pyrite; (e) Abarite in the source rocks; (f) Some euhedral-subhedral granular pyrites and mildew spherical pyrites in the source rocks. Sp sphalerite, Ga galena, Py pyrite, Sd siderite, Brt barite.

5.3. Metal Sulfide Minerals in Bitumen

Through SEM and energy spectrum analysis of the interiors of bitumen from Pb–Zn ores, abundant micro-sized galena, sphalerite, and pyrite can be identified in the inner bitumen. Among them, the galena is a rectangle (7.0 μm × 12.7 μm) and irregular granular

($0.8\ \mu\text{m} \times 1.7\ \mu\text{m}$ – $1.7\ \mu\text{m} \times 2.3\ \mu\text{m}$) in shape (Figure 9a–c), while sphalerite is cubic ($10.0\ \mu\text{m} \times 10.0\ \mu\text{m}$ – $55.0\ \mu\text{m} \times 60.0\ \mu\text{m}$) (Figure 9d,e); pyrite is mostly irregular granular ($2.8\ \mu\text{m} \times 3.3\ \mu\text{m}$) or nearly cubic ($1.6\ \mu\text{m} \times 1.6\ \mu\text{m}$) (Figure 9f), they occur in pores or as inclusions in the interiors of the bitumen.

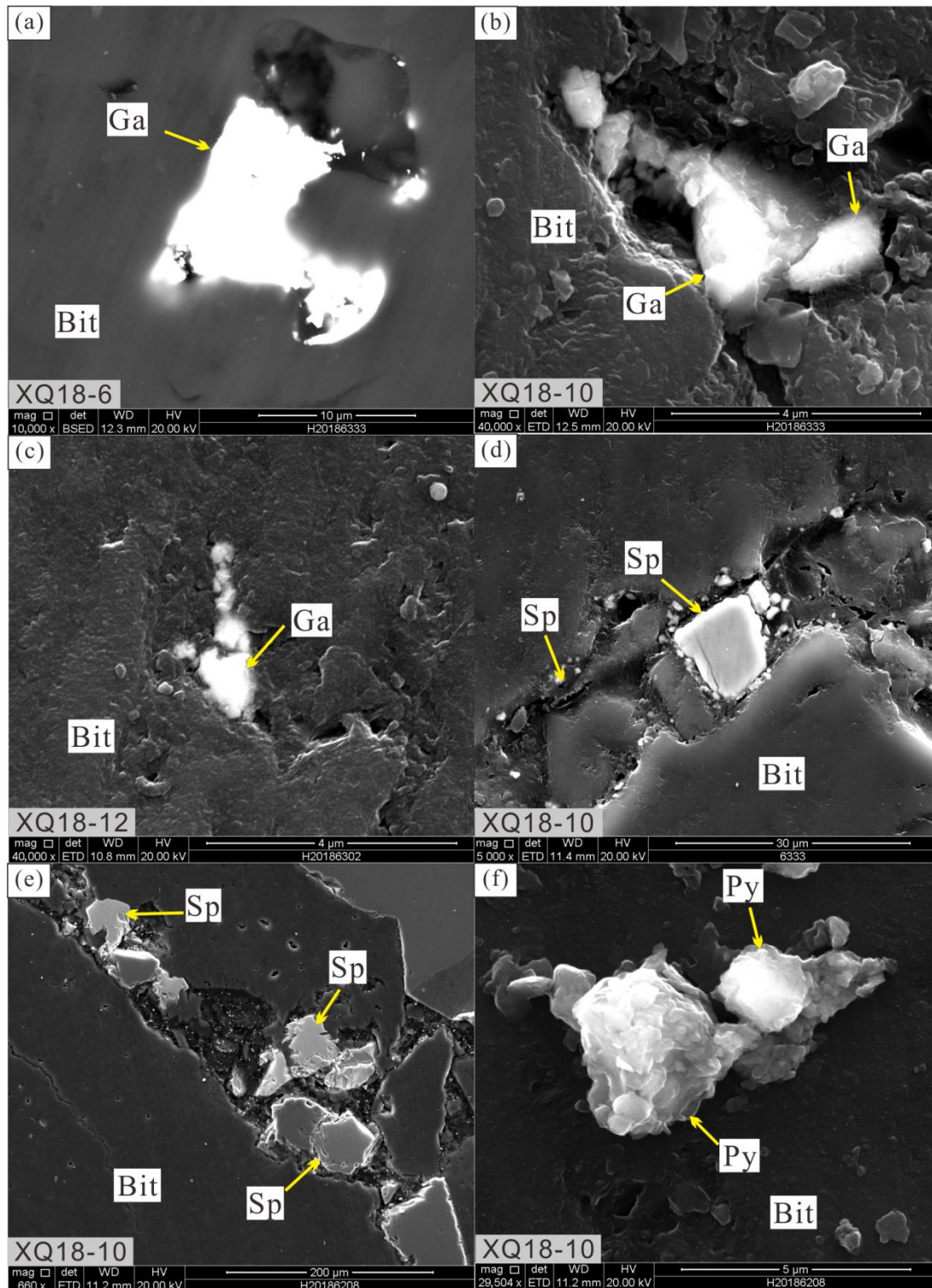


Figure 9. SEM and energy spectrum analytical results of bitumen (Bit) in paleo-oil/gas reservoirs at Xuequ. (a–c) Some galenas in the bitumen; (d,e) Some sphalerites in the bitumen; (f) Some pyrites in the bitumen. Sp sphalerite, Ga galena, Py pyrite, Bit bitumen.

5.4. Bitumen Inclusions in Sulfide Minerals

As mentioned above, most of the sphalerites that formed in the late stage of mineralization have a concentric banded structure due to differences in color and abundance of opaque inclusions. Raman spectroscopy analysis for opaque inclusions in different bands presents characteristic Raman spectral peaks of bitumen with peaks of 1319 cm^{-1} and 1606 cm^{-1} (Figure 3e,g,h). In addition, some bituminous dolostone and bitumen are encapsulated in late sphalerite (Sp_2) (Figure 5c,d). Bitumen inclusions are also found in some galena. Sphalerite and galena are rich in bitumen inclusions and host rocks with bitumen, suggesting that sphalerite and galena were formed after the thermally cracked bitumen.

5.5. Bitumen Inclusions in Quartz

Euhedral conical quartz (Q_2) with a banded structure that is paragenetic with galena (Ga_2) and sphalerite (Sp_2) is selected for inclusion in petrographic observations and Raman spectroscopy analysis. Single-phase hydrocarbon inclusions and gas–liquid two-phase aqueous inclusions are common in this kind of quartz. The bands are mainly composed of layers rich in opaque mineral inclusions and layers without inclusions distributed alternatively. Raman spectroscopy analysis of dark opaque mineral inclusions in the band shows typical Raman spectral peaks of 1328 cm^{-1} and 1602 cm^{-1} that are characteristic of bitumen, indicating that these opaque minerals are mainly bitumen inclusions (Figure 5h,i). The presence of hydrocarbon and bitumen inclusions in quartz suggests that quartz crystallized after the thermally cracked bitumen.

5.6. Sulfur Isotopic Characteristics

Single mineral grains of late galena (Ga_2) and sphalerite (Sp_2) were selected for bulk sulfur isotope analysis, and the analytical results are listed in Table 3. The $\delta^{34}\text{S}$ values of galena are 5.2‰ – 15.1‰ , with an average of 9.9‰ . The $\delta^{34}\text{S}$ values of sphalerite are between 9‰ and 18.3‰ , with an average of 12.0‰ . The $\delta^{34}\text{S}$ values of sphalerite are higher than those of galena.

Table 3. Sulfur isotope analytical results of metal sulfide minerals.

Sample Number	Location	Texture	Structure (Stage)	Mineral	$\delta^{34}\text{S}$ (‰)
SDY-3-2-G	Shandouya	Coarse grain	Laminated (II)	Galena	10.5
SDY-3-3-G	Shandouya	Coarse grain	Massive (II)	Galena	9.0
SDY-3-7-G	Shandouya	Coarse grain	Massive (II)	Galena	9.0
SDY-3-8-G	Shandouya	Coarse grain	Massive (II)	Galena	10.2
SDY-3-12-G	Shandouya	Fine grain	Disseminated (II)	Galena	8.7
XQ-1-11-G	Xuequ	Coarse grain	Massive (II)	Galena	7.9
XQ-1-42-G	Xuequ	Fine grain	Banded (II)	Galena	9.7
XQ-1-45-G	Xuequ	Medium grain	Disseminated (II)	Galena	5.4
XQ-1-47-G	Xuequ	Fine grain	Massive (II)	Galena	15.1
XQ-1-8-G	Xuequ	Fine grain	Banded (II)	Galena	5.2
XQ-1-10-G	Xuequ	Fine grain	Massive (II)	Galena	11.0
SDY-3-2-S	Shandouya	Fine grain	Laminated (II)	Sphalerite	16.8
SDY-3-3-S	Shandouya	Coarse grain	Massive (II)	Sphalerite	12.6
SDY-3-4-S	Shandouya	Fine grain	Veined (II)	Sphalerite	10.5
SDY-3-7-S	Shandouya	Coarse grain	Massive (II)	Sphalerite	12.5
SDY-3-8-S	Shandouya	Coarse grain	Massive (II)	Sphalerite	13.0
SDY-3-10-S	Shandouya	Coarse grain	Disseminated (II)	Sphalerite	11.9
SDY-3-12-S	Shandouya	Fine grain	Disseminated (II)	Sphalerite	12.9
XQ-1-8-S	Xuequ	Fine grain	Banded (II)	Sphalerite	11.3
XQ-1-11-S	Xuequ	Medium grain	Massive (II)	Sphalerite	10.7
XQ-1-13-S	Xuequ	Fine grain	Disseminated (II)	Sphalerite	12.3
XQ-1-16-S	Xuequ	Coarse grain	Banded (II)	Sphalerite	12.8
XQ-1-42-S	Xuequ	Coarse grain	Banded (II)	Sphalerite	10.5

Table 3. Cont.

Sample Number	Location	Texture	Structure (Stage)	Mineral	$\delta^{34}\text{S}$ (‰)
XQ-1-45-S	Xuequ	Coarse grain	Disseminated (II)	Sphalerite	9.0
XQ-1-33-S	Xuequ	Coarse grain	Banded (II)	Sphalerite	9.2
XQ-1-47-S	Xuequ	Coarse grain	Massive (II)	Sphalerite	18.3
XQ-1-20-S	Xuequ	Coarse grain	Disseminated (II)	Sphalerite	12.8

6. Discussion

6.1. Oil Source of Paleo-Oil and Paleo-Gas Reservoirs

Studies show that the oil sources of the paleo-oil/gas reservoirs in the Dengying Formation in the Sichuan Basin are mainly from the early Cambrian Qiongzhusi Formation shale [41–44]. The sedimentary environment, parent material source, and maturity of the bitumen from Pb–Zn ore bodies at Wusihe and the potential source rocks from the Qiongzhusi Formation in the central Sichuan Basin were chosen to compare and determine the oil source in the Wusihe paleo-oil/gas reservoirs.

(1) Sedimentary environment

$\text{Pr}/\text{Ph} < 1$ is usually considered to be a reducing environment and is mostly related to anoxic and hypersaline environments [49–51]. The Pr/Ph ratios of the Qiongzhusi Formation source rocks and bitumen were 0.54–0.85 and 0.23–0.89, respectively, and they show similarly reduced and supersaline environments.

The tricyclic diterpenes of the Qiongzhusi Formation source rocks were characterized by a $\text{C}_{23}\text{TT} > \text{C}_{21}\text{TT} > \text{C}_{20}\text{TT}$ ascending configuration, indicating that the parent material of organic matter in the Qiongzhusi Formation source rocks was mainly from seawater with high salinity [52]. The tricyclic diterpenes of the bitumen exhibited ascending configuration characteristics of $\text{C}_{23}\text{TT} > \text{C}_{21}\text{TT} > \text{C}_{20}\text{TT}$ that were similar to those of the source rocks (Figure 6).

Abundant gammacerane and a high gammacerane/ $\alpha\beta$ -hopane ratio implied strong reduction conditions and a hypersaline environment of organic matter deposition [49,53]. The higher gammacerane and higher gammacerane/ $\alpha\beta$ -hopane ratios (0.15–0.20) of the bitumen from the ore body suggested a hypersaline organic matter deposition, which was further confirmed by the abundant pregnane and homopregnane [54] (Figure 7).

(2) Parent source of organic matter

$\text{Pr}/\text{nC}_{17} > 1$ is considered algal input, but it is also related to maturity and hydrocarbon expulsion [50,51]. The Pr/nC_{17} values in both source rocks from the Qiongzhusi Formation and reservoir bitumen in the study area were lower than 1 (Table 1), which may be related to high maturation.

The organic matter type of the source rocks is sapropelic (type I) [52]. The preponderance of C_{27} steranes and C_{28} steranes indicated that the parent source of the organic matter was lower plankton and bacteria [49,53]. Abundant steranes were detected in the source rock extract, the contents of C_{27} , C_{28} , and C_{29} regular steranes were higher, and the preponderance of C_{27} steranes was obvious [52].

The C_{27} , C_{28} , and C_{29} sterane contents in the reservoir bitumen in the study area were generally high (Figure 5); the C_{29} sterane contents (0.35–0.38) were similar to those of C_{27} sterane (0.32–0.36), while the contents of C_{28} sterane were 0.27–0.34 (Table 2), which suggests a certain amount of low aquatic organisms and algae input. The 4-methyl sterane likely originated from 4-methyl alcohol in Dinophyceae organisms [55]. Abundant 4-methyl sterane was detected in all bitumen samples, which further confirms the source of the algal parent material.

(3) Maturity of organic matter

The source rocks reached the over-mature evolution stage, as indicated by the Ro value from 2.0% to 4.0% and Tmax greater than 400 °C, and can mainly generate gaseous

hydrocarbons [52]. The Ro value of the reservoir bitumen in Dengying Formation is 2.62%–4.05% (average 3.47%) [52], which belongs to over-mature pyrobitumen [43,46,47].

Carbon preference index (CPI) and OEP in the biomarker spectrum are important parameters of the maturity of organic matter [53]. The CPI and OEP values of the source rocks were 1.0–1.58 (average: 1.3) and 0.95–1.2 (average: 1.02), respectively [52]. The CPI values of the reservoir bitumen ranged from 0.99 to 1.25, with an average of 1.16, and the OEP values of the reservoir bitumen ranged from 1 to 1.36, with an average of 1.15 (Table 1). The CPI and OEP values of both source rocks and reservoir bitumen were similar, indicating that they had the same maturity.

Ts/(Ts + Tm), C₃₁ terpane 22S/(22S + 22R), and C₃₂ terpane 22S/(22S + 22R) in the biomarker spectrum are commonly used to determine the degree of the thermal evolution of organic matter. With the increasing maturity of organic matter, the ratio of 22S/(22S + 22R) increased from 0 to approximately 0.6 (the equiponderant state varies from 0.57 to 0.6) [53]. The Ts/(Ts + Tm), C₃₁ 22S/(22S + 22R), and C₃₂ 22S/(22S + 22R) of the source rocks from the Qiongzhusi Formation were 0.35–0.56 (average: 0.46), 0.51–0.56 (average: 0.54) and 0.54–0.58 (average: 0.56), respectively [52]. The Ts/(Ts + Tm), C₃₁ 22S/(22S + 22R), and C₃₂ 22S/(22S + 22R) of the reservoir bitumen were 0.45–0.51 (average: 0.46), 0.54–0.55 (average: 0.54) and 0.57–0.59 (average: 0.58), respectively (Table 2). The maturity parameters from the terpane of both source rocks and reservoir bitumen were similar, indicating that they had a similar thermal evolutionary history.

The molecular parameters C₂₉ββ/(αα + ββ) and C₂₉αα20S/(20S + 20R) of steranes are commonly used maturity parameters [53]. The C₂₉ββ/(αα + ββ) and C₂₉αα20S/(20S + 20R) values of the source rocks from the Qiongzhusi Formation were 0.36–0.49 and 0.8–0.47, with average values of 0.43 and 0.42, respectively [52]. The C₂₉ββ/(αα + ββ) and C₂₉αα20S/(20S + 20R) values of the reservoir bitumen were 0.36–0.43 and 0.38–0.45, with average values of 0.39 and 0.42 (Table 2), respectively. Both source rocks and reservoir bitumen had similar C₂₉ββ/(αα + ββ) and C₂₉αα20S/(20S + 20R) values, indicating that they had similar maturities.

From the above analysis, the formation environment, parent material source, and maturity of the organic matter from the source rocks in the Qiongzhusi Formation and reservoir bitumen in the Maidiping Member are readily compared, indicating that the oil source of bitumen is mainly from the source rocks of the Qiongzhusi Formation.

6.2. Formation and Evolution Process of the Paleo-Oil and Paleo-Gas Reservoirs

Studies show that the oil/gas reservoirs of the Dengying Formation in the Sichuan Basin have similar hydrocarbon accumulation processes; there are two peaks of oil accumulation and one peak of thermal cracking gas generation [41,43,56]. With the increase in the burial depth, the lower Cambrian Qiongzhusi Formation reached the thermal peak for oil generation, and oil accumulated to form early paleo-oil reservoirs at 458.09 ± 5.59 Ma in the northern margin of the basin [56,57], 486 ± 15 Ma in the northwestern margin of the basin [56,57] and 414 ± 15 Ma in the depocenter areas of the central basin [43] (Figure 10). Then, as the source rock of the Qiongzhusi Formation was buried deeply again during the Late Triassic, the source rocks reached the thermal peak for oil generation to form late oil/gas reservoirs in the northern margin and central areas of the Sichuan Basin. In the central Sichuan Basin, source rocks in the more shallowly buried parts passed through the peak thermal window for oil formation, which migrated together with the oil generated at 414 ± 15 Ma into the reservoirs to form late paleo-oil reservoirs; meanwhile, source rocks in the basin depocenter generated gas due to their high maturity (Figure 10) [43,58], suggesting that the late paleo-oil reservoirs in the central Sichuan Basin were formed at 220–205 Ma. After the formation of the late paleo-reservoirs, as the paleo-oil reservoirs were deeply buried, the paleo-oil reservoirs reached the threshold for the thermal cracking of oil and underwent in situ thermal cracking to form overpressure paleo-gas reservoirs [59] and thermally cracked bitumen (pyrobitumen) [41,47,59]; however, there was some dispute about the time of transformation from the paleo-oil reservoirs to paleo-gas reservoirs in

the Sichuan Basin. On the northern margin of the basin, the Re–Os isotopic dating of pyrobitumen gives ages of paleo-gas reservoirs generation of approximately 205 ± 32 Ma, 184 ± 23 Ma, and 173 ± 12 Ma [56,57]; among them, 184 ± 23 Ma was suggested as the most likely age of paleo-gas reservoirs generation [56]. In the central Sichuan Basin, the Re–Os isotopic dating of pyrobitumen suggested ages of 78 ± 37 Ma [43] and 154 ± 21 Ma [58], which are much later than those in the northern margin. Because the transformation from paleo-oil reservoirs to paleo-gas reservoirs is continuous, according to the generation time of paleo-oil reservoirs of approximately 220–205 Ma, which was suggested by Su et al. (2022) [58], 205 Ma is the most likely age of paleo-gas reservoirs generation in the central Sichuan Basin, and this age is also consistent with the generation time of paleo-gas reservoirs in the northern margin of the basin. The ages of 78 ± 37 Ma and 154 ± 21 Ma may be the times of paleo-gas reservoirs adjustment. During the late Indosinian–Himalayan period, the paleo-gas reservoirs began to adjust from overpressure gas reservoirs to the present normal-pressure gas reservoirs [59]. These gas reservoirs were preserved only in the central Sichuan Basin and destroyed around the Sichuan Basin periphery areas, where Pb–Zn deposits have been found.

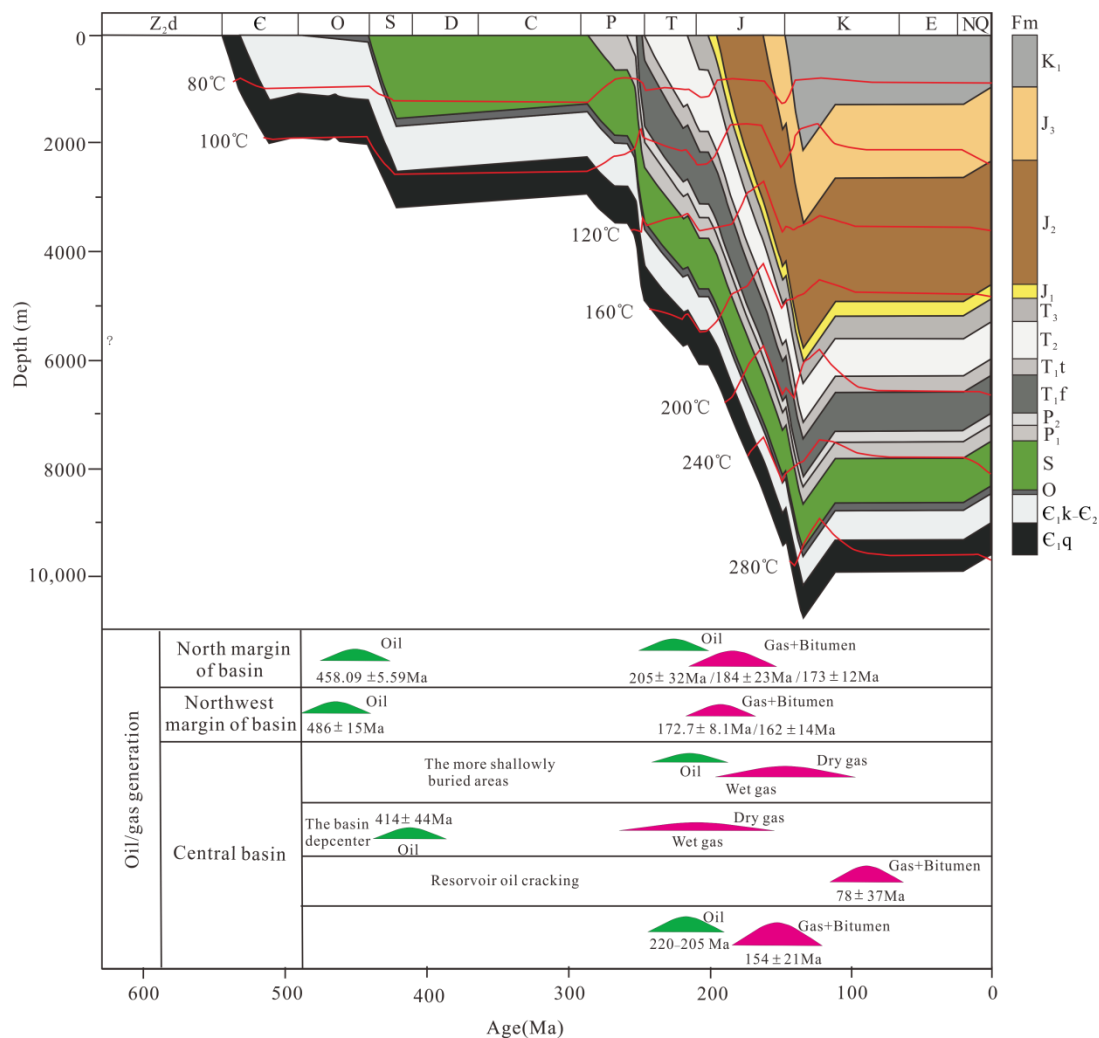


Figure 10. The burial history of source rocks and hydrocarbon accumulation times. The ages of oil/gas generation in the northern and northwestern margins of the Sichuan Basin are from Shen et al. (2019) [56] and Ge et al. (2018) [57], and those in the central Sichuan Basin are from Shi et al. (2020) [43] and Su et al. (2020, 2022) [58,60].

6.3. Times of Mineralization and Hydrocarbon Accumulation

Based on Rb–Sr isotope dating of six sphalerite samples from the Heiqu, Xuequ, and Shandouya, Xiong et al. (2018) [31] obtained a metallogenic age of 411 ± 10 Ma, which was similar to the early paleo-oil reservoir generation age of 414 Ma in the central Sichuan Basin [43] but far from the generation time of the paleo-gas reservoirs in the northern margin and central part of the basin.

Studies show that the metallogenic ages of MVT Pb–Zn deposits in the western margin of the Yangtze Block are relatively concentrated, and most of the deposits formed at approximately 200 Ma. For example, in Sichuan Province, the Mayuan Pb–Zn deposit and the Paomashan Pb–Zn deposit formed at 206.0 ± 6.5 Ma [7] and 200.1 ± 4 Ma [61], respectively. In Yunnan Province, the Huize Pb–Zn deposit, Lehong Pb–Zn deposit, Qiaojia Pb–Zn deposit, and Jinshachang Pb–Zn deposit formed at 222 ± 14 Ma [62], 200.9 ± 8.3 Ma [63], 196 ± 13 Ma [64] and 200.1 ± 1.6 Ma [6], respectively. The Tianqiao Pb–Zn deposit in Guizhou Province formed at 191.9 ± 6.9 Ma [65]. Recently, we selected the late sphalerite (Sp₂) of the Pb–Zn ore body in the Wusihe area for Rb–Sr isotope dating and obtained a mineralization age of 202.2 ± 4.8 Ma (discussed in a future paper). These metallogenic ages are consistent with the formation time of 205 ± 32 Ma for the paleo-gas reservoirs in the northern margin of the basin and 205 Ma for the paleo-gas reservoir in the central Sichuan Basin.

The petrographic observations of the Wusihe Pb–Zn deposits showed the coexistence of galena (Ga₂), sphalerite (Sp₂), quartz (Q₂), and bitumen (Bit₂). The quartz (Q₂) that is paragenetic with galena and sphalerite is rich in hydrocarbons, bitumen (pyrobitumen), and gas–liquid brine inclusions, while gas–liquid brine inclusions occur in sphalerite. The homogenization temperatures of fluid inclusions in quartz (Q₂) and sphalerite (Sp₂) are mainly concentrated in the range of 140–280 °C [29]. The homogenization temperatures of quartz (Q₂) and sphalerite (Sp₂) are within the thermal cracking temperature of oil, indicating that the bitumen coexisted with sphalerite and quartz and that the bitumen inclusions in sphalerite should be thermally cracked bitumen (i.e., pyrobitumen). All these facts indicate that large-scale mineralization in the study area occurred during the transformation from paleo-oil reservoirs to paleo-gas reservoirs or during the process of the adjustment-destruction of paleo-gas reservoirs. The facts such as consistency between the metallogenic age (202.2 ± 4.8 Ma) and the generation age of paleo-gas reservoirs (205 Ma) and pyrobitumen inclusions in sphalerite suggest a close genetic relationship between mineralization and accumulation or destruction of the paleo-gas reservoirs. Therefore, the mineralization of the Wusihe Pb–Zn deposits may have occurred during the transformation process from the paleo-oil reservoirs to the paleo-gas reservoirs in the Indosinian period or during the adjustment and accumulation or destruction process of the paleo-gas reservoirs.

6.4. Sources of Ore-Forming Metal Elements

It is a disputable issue for the sources of the ore-forming metal elements in the Wusihe Pb–Zn deposits. The basement, host rock, and seawater [30–33] or the Qiongzhusi Formation source rock [35] have the potential to contribute to the metals available for mineralization. Previous oil source analysis of reservoir bitumen in the Pb–Zn deposits shows that the oil source of paleo-oil/gas reservoirs was mainly from the Cambrian Qiongzhusi Formation. Pb and Zn contents in some source rocks of the Qiongzhusi Formation in the northern, southwestern, and central parts of the Sichuan Basin are within 19.8–132 ppm and 81–662 ppm, respectively; and are abnormally higher than the Clark value of the crust (Pb: 15 ppm, Zn: 76 ppm) [35]. At the same time, micron-sized galena, sphalerite, pyrite, and barite are present in the source rocks, indicating that the source rocks have the capacity to provide metal elements for mineralization, while basement rocks may be the important contributors of metal elements in Qiongzhusi Formation [35]. The SEM and energy spectrum analysis of the source rocks at Xuequ show that there are micron-sized galena, sphalerite, pyrite, and barite in the source rocks (Figure 8). The high contents of Pb and Zn [35] and the presence of micron-sized sulfide minerals in some source rocks at

Xuequ indicate that the source rocks of the Qiongzhusi Formation have the potential to supply metal elements for mineralization.

Studies have shown that ore-forming metal elements are not only enriched in crude oil or oilfield brine but enriched in solid organic matter (bitumen) through the migration of metal–organic complexes [22]. The average contents of Pb and Zn in world crude oil are 0.2–0.5 ppm and 0.5–6 ppm, respectively [27]. In oilfield brines from the Pleasant Bayou, Texas, and the Rayleigh Field, Central Mississippi, USA, concentrations of Pb are 0.4–1.1 ppm and 17–111 ppm, respectively, and concentrations of Zn are 1.5–1.6 ppm and 33–367 ppm, respectively [25]. The Pb and Zn contents in the bitumen of the Magmont Pb–Zn deposit in Missouri are 150 ± 25 ppm and 1000 ± 250 ppm, respectively [9]. The analysis of Pb and Zn contents in the bitumen of the Xuequ Pb–Zn mine shows that the Pb and Zn contents of 12 bitumen samples are within 20–287 ppm (average: 95.8 ppm) and 15–5370 ppm (average: 543.4 ppm) (Table 4); the average contents of lead and zinc are 6.4 and 7.2 times the crustal Clark value, respectively. The SEM and energy spectrum analysis for the bitumen show that micron-sized galena, sphalerite, and pyrite are present in the interior of the bitumen (Figure 9). The abnormally high contents of Pb and Zn and the occurrence of micron-sized sulfide mineral crystals in the bitumen indicate that the metal elements required for mineralization are abnormally enriched in crude oil.

Table 4. Analytical results of ore-forming metal elements in bitumen from the Xuequ Pb–Zn mine (ppm) (according to Tan et al., 2021 [35]).

Sample Number	Pb	Zn
XQ-18-2	287	15
XQ-18-3	52	21
XQ-18-6	152	36
XQ-18-7	85	40
XQ-18-9	20	67
XQ-18-13	31	75
XQ-18-21	42	76
XQ-18-23	143	102
XQ-18-27	86	231
XQ-18-31	58	232
XQ-18-36	63	256
XQ-18-38	131	5370

Studies have shown that in the process of MVT Pb–Zn mineralization, when the Pb content reaches 2.0×10^{-6} and the Zn content reaches 1.3×10^{-6} in the ore fluid, mineralization can occur [27]. The Pb and Zn contents in bitumen (Table 4) are much higher than those required for mineralization, indicating that oil may be an initial ore fluid. The abnormally high contents of Pb and Zn in the source rocks and the existence of micron-sized galena and sphalerite indicate that the ore-forming metal elements may have been pre-enriched in the source rocks under the action of organic matter. In the process of the deep burial of the source rocks, the ore-forming metal elements are separated from the source rocks. As the ore-transporting agents of metallogenic metal elements, oil carrying abundant ore-forming metal elements migrated from the source rocks to the trap and accumulated to form paleo-oil reservoirs, so the oils have the potential to contribute to the metals available for mineralization.

The grain size difference between the micron-sized galena and sphalerite crystals in the bitumen and the millimeter- to centimeter-sized galena and sphalerite crystals in the present ore bodies implies that mineralization did not take place during the development of the paleo-oil reservoir, but instead, large-scale mineralization occurred during the transformation process from the paleo-oil reservoir to the paleo-gas reservoir or the adjustment–destruction process of the paleo-gas reservoir. This process can also be sup-

ported by the thermally cracked bitumen in the galena and sphalerite and the fluid inclusion homogenization temperature of sphalerite.

6.5. Sources of Ore-Forming Sulfur

There are mainly three sources of sulfur in hydrothermal mineralization [66–68]: (a) mantle source with values of $\delta^{34}\text{S} \approx 0$, but mostly $0\text{‰} \pm 3\text{‰}$; (b) seawater sulfur source [69], for which the specific sulfur isotope value depends on the $\delta^{34}\text{S}$ values of marine evaporite in the strata [69]; and (c) biological sources of sulfur, which usually have negative $\delta^{34}\text{S}$ values.

The $\delta^{34}\text{S}$ values of sulfide minerals in the study area range from 5.2‰ to 18.3‰, with an average of 11.1‰. The $\delta^{34}\text{S}$ values of sphalerite (average 12.0‰) are higher than those of galena (average 9.9‰). In the condition of sulfur isotopic equilibrium, $\delta^{34}\text{S}_{\text{ZnS}} = \delta^{34}\text{S}_{\text{H}_2\text{S}} + (0 \sim +1\text{‰})$, $\delta^{34}\text{S}_{\text{PbS}} = \delta^{34}\text{S}_{\text{H}_2\text{S}} + (0 \sim -5\text{‰})$, so the sulfide will show the characteristics of $\delta^{34}\text{S}_{\text{ZnS}} > \delta^{34}\text{S}_{\text{PbS}}$ [66], the $\delta^{34}\text{S}$ difference between the sphalerite and galena should be ascribed to the kinetic isotopic effects. The $\delta^{34}\text{S}$ values of most samples are concentrated between 10.2‰ and 13‰ (Table 3), and the low value is close to that of mantle-derived sulfur. However, the study area lacked regional magmatic activity during the metallogenic period, so the source of mantle-derived sulfur can be excluded. The Pb–Zn ore bodies in the study area mainly occur in the Cambrian Maidiping Member. The $\delta^{34}\text{S}$ values of the early Cambrian seawater are within 25‰–33‰ [70]. The high value and average $\delta^{34}\text{S}$ value of galena and sphalerite are lower than the $\delta^{34}\text{S}$ value of early Cambrian seawater, indicating that the sulfur required for mineralization cannot be directly derived from seawater.

There are three ways to achieve the transition from SO_4^{2-} to S^{2-} in hydrothermal metallogenic systems: thermochemical sulfate reduction (TSR), bacterial sulfate reduction (BSR), and thermal decomposition of organic compounds (DOC) [71–74].

BSR reactions generally occur at low temperatures of 30–40 °C [75]. The homogenization temperatures of fluid inclusions of quartz, calcite, and dolomite that are paragenetic with galena and sphalerite are mainly concentrated within 140–280 °C [29], which is much higher than the temperature required for the BSR reaction. Therefore, the sulfur required for mineralization is unlikely to be generated through the BSR reaction.

Since mineralization in the study area mainly occurs at higher temperatures, the thermal decomposition of organic compounds at this temperature is mainly characterized by the thermal cracking of petroleum. The $\delta^{34}\text{S}$ values of sulfur from oil or other organic matter are usually within 4‰–8.9‰ [76]. However, the hydrogen sulfide content formed by the thermal decomposition of organic compounds is very limited, usually less than 3% [77]. Therefore, the thermal decomposition of petroleum can provide a certain amount of sulfur for mineralization, but the amount that is provided is very limited.

TSR usually occurs at temperatures higher than 125 °C [78]. The homogenization temperatures of fluid inclusions in both sphalerite and paragenetic quartz in the study area are higher than 125 °C [29], and gypsum exists in the ore-bearing strata in the adjacent area. The ore-forming area is also located in paleo-oil/gas reservoirs. All the conditions required for the TSR reaction are available. Assuming that sulfur is mainly derived from early Cambrian evaporites with $\delta^{34}\text{S}$ values between 25‰ and 33‰ [70], the TSR reaction at 200–100 °C can produce 10‰ to 20‰ isotopic fractionation between sulfates and sulfides [75,79,80]. The theoretically predicted $\delta^{34}\text{S}$ values (from 5‰ to +23‰) are in good agreement with the observed $\delta^{34}\text{S}$ values (from 5.2‰ to 18.3‰) of sulfide minerals. Therefore, we believe that the sulfur source required for mineralization is mainly provided by TSR. Previous studies have also confirmed the existence of TSR in the process of mineralization [29,33,34].

In conclusion, although some hydrogen sulfide can be formed by the thermal cracking of petroleum, the amount of hydrogen sulfide is very limited, and the sulfur source for mineralization mainly comes from the hydrogen sulfide provided by the TSR reaction.

6.6. Relationship between Mineralization and Accumulation

The analysis of results obtained in this study shows that thermally cracked bitumen is present in the Wusihe MVT Pb–Zn deposit, and the ore bodies mainly occupy the upper part of the paleo-gas reservoir. The galena and sphalerite coexisted with the thermally cracked bitumen and were superimposed spatially. The Cambrian Qiongzhusi Formation is not only the source rocks of the paleo-oil/gas reservoirs but also the source bed of the MVT Pb–Zn deposit.

Organic compounds generally contain a considerable number of hydrophilic functional groups, which can chelate with a variety of metal ions to form soluble complexes for migration [81]. The porphyrins are extractable, organic chelating species, within which a central metal ion is coordinated with four nitrogen atoms, which form part of a porphyrin ring structure as part of a tetrapyrrole complex; it is assumed that the behavior of the porphyrins with respect to metal complexation is representative of metal complexation by analogous tetrapyrrole complexes within nonporphyrin species [27]. The organic coordination groups and Pb and Zn may form a stable soluble metal–organic complex with good thermal stability in aqueous solution [82,83]. Therefore, with the maturation of organic matter and the formation of oil, metal ions, such as Pb and Zn, in source rocks chelate with organic compounds to form soluble metal–organic complexes [27,28]. The discovery of ore-forming metal elements, sulfide minerals in bitumen, and sulfide minerals in source rocks, as well as the content of ore-forming elements in some bitumen, is much higher than the contents of Pb and Zn required for mineralization, indicating that oil is not only the ore-transporting agent of metallogenic metal elements but also provides the metals available for mineralization.

Metal elements are usually incorporated with porphyrins or other organic species in oil to form metal–organic complexes [27]. They migrated with oil into traps to form paleo-oil reservoirs, where metal elements existed as organic complexes in paleo-oil reservoirs. Because the sulfide minerals in the bitumen in the study area are mostly micron-sized, they are very different from the millimeter- to centimeter-sized sulfide minerals in the present ores. At the same time, the homogenization temperatures of fluid inclusions in sphalerite and gangue minerals (140–280 °C) [29], as well as the presence of a large number of thermally cracked bitumen inclusions in sphalerite, together indicate that large-scale Pb–Zn mineralization occurred after the paleo-oil reservoirs were formed. With the deep burial of the paleo-oil reservoirs with abundant Pb–Zn metal elements, the bond between the metal and organic ligands in the paleo-oil reservoir was broken during the in situ transformation of paleo-oil reservoirs to form the paleo-gas reservoirs, resulting in the decoupling of metal elements and organic matter. The decoupled metal elements were carried in the oilfield brine underlying the paleo-gas reservoirs. At the same time, a large amount of H₂S was formed by TSR, and minor H₂S was generated by the thermal cracking of petroleum or decomposition of the organic matter; they were dissolved into oilfield brine around the gas–water interface under an overpressured environment [84] to form ore-forming fluid rich in metal elements of Pb and Zn and H₂S.

Studies based on the hydrocarbon accumulation process of the present gas reservoirs in the Dengying Formation in the central Sichuan Basin concluded that they underwent decompression adjustment and accumulation from overpressure to normal pressure [41,59,84]. During this process, as the pressure decreased, the paleo-gas–water interface migrated upward, and the bottom water of the oilfield underlying the paleo-gas reservoirs entered into the pores and caves evacuated by the natural gas to precipitate, resulting in the development of quartz, calcite, dolomite, bitumen (Bit₂) and minor sphalerite. Among the aforementioned minerals, calcite, quartz, and sphalerite were characterized by abundant bitumen and methane inclusions [59,84]. A comparative study revealed that the study area had an accumulation process similar to that of the central Sichuan area before they were destroyed. The process of mineralization and hydrocarbon accumulation in the study areas can be summarized as shown in Figure 11.

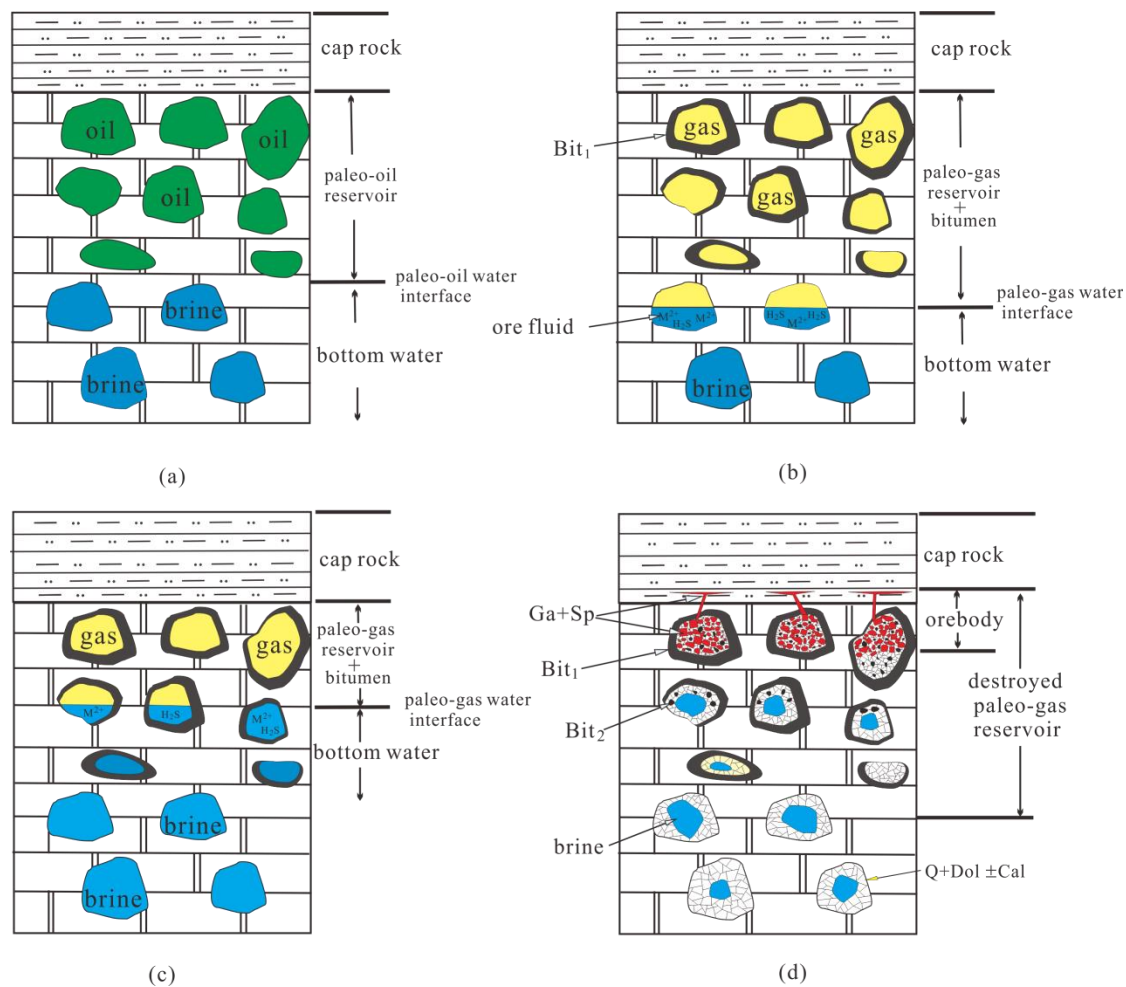


Figure 11. Schematic diagram of hydrocarbon accumulation and mineralization processes. (a) Petroleum is the initial ore-forming fluid, and hydrocarbons accumulated to form the paleo-oil reservoir; (b) In situ thermal cracking of the paleo-oil reservoir formed an overpressure paleo-gas reservoir, hydrogen sulfide was formed by TSR, and metal elements were decoupled from organic matter to form ore fluid around the gas–water interface; (c) The paleo-gas reservoir was destroyed, and the gas–water interface migrated upward. The ore fluid and oilfield brine migrated upward to the space after the escape of the paleo-gas reservoir; (d) The paleo-gas reservoir was completely destroyed, and the ore fluid mineralized to form ore minerals (galena and sphalerite) and gangue minerals (quartz, dolomite, bitumen, and calcite). Ga galena, Sp sphalerite, Bit bitumen, Q quartz, Dol dolomite, Cal calcite, M^{2+} metal ions.

With the maturity of organic matter in source rocks, the ore-forming metal elements (in the form of metal–organic complexes) and hydrocarbons were expelled from the source rocks and accumulated in the Maidiping Member to form paleo-oil reservoirs (Figure 11a); during this process, the source rocks provided not only the oil source for the paleo-oil reservoirs but also the metal source for the mineralization, and the oil acted as an ore-transporting agent for the metals. After the paleo-oil reservoirs were formed, the paleo-oil reservoirs were buried and reached the threshold for the thermal cracking of oil. They underwent in situ thermal cracking to form overpressure paleo-gas reservoirs and a large amount of bitumen. The metal elements, such as Pb and Zn, and the organic matter were decoupled because the bond between the metals and organic ligands was broken and entered into the oilfield brine around the gas–water interface. At the same time, H_2S was formed by the TSR, and the minor thermal cracking of oil occurred. They dissolved into brines around the gas–water interface and formed an ore-forming fluid layer rich in metal

elements and H₂S (Figure 11b). Subsequently, the paleo-gas reservoirs were destroyed, and the ore fluid around the gas–water interface and the oilfield brine far away from the gas–water interface successively migrated upward into the paleo-gas reservoirs and occupied the pore spaces and cavities left behind by natural gas escape (Figure 11c). The ore-forming fluids and oilfield brine precipitated to form lead–zinc ore bodies and other hydrothermal minerals as sudden pressure relief of the overpressure paleo-gas reservoirs occurred (Figure 11d), resulting in special spatiotemporal associated or paragenetic relations of galena, sphalerite, and bitumen.

7. Conclusions

- (1) The MVT Pb–Zn deposit and paleo-oil/gas reservoirs in the dolomite of the Maidiping Member are distributed along the paleokarst interface between the Maidiping Member and the Qiongzhusi Formation; they overlap spatially, and the Pb–Zn ore bodies mainly occupy the upper part of the paleo-oil/gas reservoirs. Both the Pb–Zn ore and sphalerite are rich in thermally cracked bitumen with μm -sized crystals of galena and sphalerite, of which contents of lead and zinc are higher than those required for Pb–Zn mineralization.
- (2) The oil source of the paleo-oil reservoirs from the Cambrian Qiongzhusi Formation not only provided oil sources for paleo-oil reservoirs but also provided ore-forming metal elements for Pb–Zn mineralization.
- (3) The oil may act as an ore-transporting agent for metallogenic metal elements. Liquid oil with abundant ore-forming metals accumulated to form paleo-oil reservoirs with mature organic matter in source rocks. As paleo-oil reservoirs were buried, the oil underwent in situ thermal cracking to form overpressure paleo-gas reservoirs and a large amount of bitumen. The generation time of the paleo-gas reservoirs is similar to the metallogenic time.
- (4) The metal elements that were decoupled from organic matter and H₂S that formed by TSR and minor decomposition of the organic matter dissolved in oilfield brine around the gas–water interface to form the ore fluid during oil thermal cracking and paleo-gas reservoir development.
- (5) The large-scale Pb–Zn mineralization is mainly related to the destruction of overpressured paleo-gas reservoirs; the sudden pressure relief caused the ore fluid around the gas–water interface to migrate upward into the paleo-gas reservoirs and induced extensive metal sulfide precipitation in the ore fluid, resulting in special spatiotemporal associated or paragenetic relations of the galena, sphalerite, and bitumen.

Author Contributions: Conceptualization, G.W.; Formal analysis, Q.L., G.L. and J.L.; Funding acquisition, G.W.; Investigation, G.W.; Methodology, G.W.; Project administration, G.W.; Resources, Q.L. and Z.H.; Software, Z.H.; Supervision, G.W.; Validation, Q.L., Z.H., Y.F. and N.L.; Visualization, Q.L. and Z.H.; Writing—original draft, G.W.; Writing—review & editing, G.W. All authors have read and agreed to the published version of the manuscript.

Funding: This research was funded by the National Natural Science Foundation of China, grant number 41773033.

Data Availability Statement: The data presented in this study are available in this paper.

Acknowledgments: We thank the anonymous reviewers and Dongyu Zheng for their constructive reviews and valuable suggestions that immensely enhanced the manuscript.

Conflicts of Interest: The authors declare no conflict of interest.

References

1. Gize, A.P.; Barnes, H.L. The organic geochemistry of two Mississippi Valley-Type Lead-Zinc deposits. *Econ. Geol.* **1987**, *82*, 457–470. [[CrossRef](#)]
2. Tompkins, L.A.; Rayner, M.J.; Groves, D.I.; Roche, M.T. Evaporites; in situ sulfur source for rhythmically banded ore in the Cadjebut Mississippi Valley-Type Zn–Pb deposit, Western Australia. *Econ. Geol.* **1994**, *89*, 467–492. [[CrossRef](#)]

3. Kesler, S.E.; Jones, H.D.; Furman, F.C.; Sassen, R.; Anderson, W.H.; Kyle, J.R. Role of crude oil in the genesis of Mississippi Valley-Type deposits: Evidence from the Cincinnati Arch. *Geology* **1994**, *22*, 609. [[CrossRef](#)]
4. Fallara, F.; Savard, M.M. A Structural, petrographic, and geochemical study of the Jubilee Zn–Pb deposit, Nova Scotia, Canada, and a new metallogenic model. *Econ. Geol.* **1998**, *93*, 757–778. [[CrossRef](#)]
5. Wu, Y.; Zhang, C.Q.; Mao, J.W.; Ouyang, H.G.; Sun, J. The genetic relationship between hydrocarbon systems and Mississippi Valley-Type Zn–Pb deposits along the SW margin of Sichuan Basin, China. *Int. Geol. Rev.* **2013**, *55*, 941–957. [[CrossRef](#)]
6. Zhang, C.Q.; Wu, Y.; Hou, L.; Mao, J.W. Geodynamic setting of mineralization of Mississippi Valley-Type deposits in world-class Sichuan–Yunnan–Guizhou Zn–Pb triangle, Southwest China: Implications from Age-Dating studies in the past decade and the Sm–Nd age of Jinshachang deposit. *J. Asian Earth Sci.* **2015**, *103*, 103–114. [[CrossRef](#)]
7. Wang, G.Z.; Huang, Z.; Zhao, F.F.; Li, N.; Fu, Y.Z. The relationship between hydrocarbon accumulation and Mississippi Valley-type Pb–Zn mineralization of the Mayuan metallogenic belt, the Northern Yangtze Block, SW China: Evidence from ore geology and Rb–Sr isotopic dating. *Resour. Geol.* **2020**, *70*, 188–203. [[CrossRef](#)]
8. Huang, Z.; Wang, G.Z.; Li, N.; Fu, Y.Z.; Lei, Q.; Mao, X.L. Genetic link between Mississippi Valley-Type (MVT) Zn–Pb mineralization and hydrocarbon accumulation in the Nanmushu, Northern Margin of Sichuan Basin, SW China. *Geochemistry* **2021**, *81*, 125805. [[CrossRef](#)]
9. Marikos, M.A.; Laudon, R.C.; Leventhal, J.S. Solid insoluble bitumen in the magmont west orebody, Southeast Missouri. *Econ. Geol.* **1986**, *81*, 1983–1988. [[CrossRef](#)]
10. Arne, D.C.; Curtis, L.W.; Kissin, S.A. Internal zonation in a carbonate-hosted Zn–Pb–Ag deposit, Nanisivik, Baffin Island, Canada. *Econ. Geol.* **1991**, *86*, 699–717. [[CrossRef](#)]
11. Macqueen, R.W.; Powell, T.G. Organic geochemistry of the Pine Point Lead–Zinc ore field and region, Northwest Territories, Canada. *Econ. Geol.* **1983**, *78*, 1–25. [[CrossRef](#)]
12. Selby, D.; Creaser, R.; Dewing, K.; Fowler, M. Evaluation of bitumen as a Re–Os geochronometer for hydrocarbon maturation and migration: A test case from the Polaris MVT deposit, Canada. *Earth Planet. Sci. Lett.* **2005**, *235*, 1–15. [[CrossRef](#)]
13. Parnell, J. Hydrocarbon minerals in the Midland Valley of Scotland with particular reference to the oil-shale group. *Proc. Geol. Assoc.* **1984**, *95*, 275–285. [[CrossRef](#)]
14. Xue, C.J.; Gao, Y.B.; Zeng, R.; Chi, G.X.; Qing, H.R. Organic Petrography and Geochemistry of the Giant Jinding Deposit, Lanping Basin, Northwestern Yunnan, China. *Acta Petrol. Sin.* **2007**, *23*, 2889–2900. Available online: http://www.ysxb.ac.cn/article/id/aps_200701119 (accessed on 20 October 2022). (In Chinese with English Abstract)
15. Hanor, J.S. The sedimentary genesis of hydrothermal fluids. In *Geochemistry of Hydrothermal Deposits*, 2nd ed.; Barnes, H.L., Ed.; John Wiley and Sons: New York, NY, USA, 1979; pp. 137–168, ISBN 0471050563.
16. Beales, F.W. Precipitation mechanisms for Mississippi Valley-Type ore deposits. *Econ. Geol.* **1975**, *70*, 943–948. [[CrossRef](#)]
17. Powell, T.G.; MacQueen, R.W. Precipitation of sulfide ores and organic matter: Sulfate reactions at Pine Point, Canada. *Science* **1984**, *224*, 63–66. [[CrossRef](#)]
18. Leach, D.L.; Sangste, D.F.; Kelley, K.D.; Large, R.R.; Garven, G.; Allen, C.R.; Gatzmer, J.; Walters, S. Sediment-hosted Lead–Zinc deposit: A global perspective. *Econ. Geol.* **2005**, *105*, 561–607.
19. Wilson, N.S.F.; Zentilli, M. Association of pyrobitumen with copper mineralization from the Uchumi and Talcuna districts, Central Chile. *Int. J. Coal Geol.* **2006**, *65*, 158–169. [[CrossRef](#)]
20. Tu, G.C. *Geochemistry of Stratigraphic Deposits in China*; Science Press: Beijing, China, 1988; Volume 3, ISBN 7-03-000486-8. (In Chinese)
21. Shi, J.X.; Yu, X.Y.; Wang, H.Y. The role of ancient oil reservoirs, Bitumens and bitumen inclusions in metallogenetic research. *Acta Mineral. Sin.* **1995**, 117–122. (In Chinese with English Abstract) [[CrossRef](#)]
22. Parnell, J. Metal enrichments in solid bitumens: A review. *Miner. Depos.* **1988**, *23*, 191–199. [[CrossRef](#)]
23. Shi, J.X.; Wang, H.Y.; Lin, Q. The relationship between the formation of gold, antimony and mercury low temperature deposits and organic matter. In *Low Temperature Geochemistry*; Tu, G.C., Ed.; Science Press: Beijing, China, 1998; pp. 53–76. (In Chinese)
24. Gu, X.X.; Zhang, Y.M.; Li, B.H.; Xue, C.J.; Dong, S.Y.; Fu, Z.H.; Cheng, W.B.; Liu, L.; Wu, C.Y. The Coupling Relationship between Metallization and Hydrocarbon Accumulation in Sedimentary Basins. *Earth Sci. Front.* **2010**, *17*, 83–105. Available online: <https://www.earthsciencefrontiers.net.cn/EN/Y2010/V17/I2/83> (accessed on 31 October 2022). (In Chinese with English Abstract)
25. Sverjensky, D.A. Oil field brines as ore-forming solutions. *Econ. Geol.* **1984**, *79*, 23–37. [[CrossRef](#)]
26. Peabody, C.E.; Einaudi, M.T. Origin of petroleum and mercury in the Culver–Baer Cinnabar deposit, Mayacmas District, California. *Econ. Geol.* **1992**, *87*, 1078–1103. [[CrossRef](#)]
27. Manning, D.A.C.; Gize, A.P. The role of organic matter in ore transport processes. In *Organic Geochemistry: Principles and Application*; Engel, M.H., Macko, S.A., Eds.; Plenum Press: New York, NY, USA, 1993; pp. 547–563, ISBN 978-1-4613-6252-4.
28. Zhuang, H.P.; Lu, J.L.; Wen, H.J.; Mao, H.H. Organic matter in hydrothermal ore-forming fluid. *Earth Environ.* **1997**, *1*, 85–91.
29. Xiong, S.F.; Yao, S.Z.; Gong, Y.J.; Tan, M.T.; Zeng, G.P.; Wang, W. Ore-forming fluid and thermochemical sulfate reduction in the Wusihe Lead–Zinc deposit, Sichuan Province, China. *Earth Sci. China Univ. Geosci.* **2016**, *41*, 105. [[CrossRef](#)]
30. Zhang, H.J.; Fan, H.F.; Xiao, C.Y.; Wen, H.J.; Ye, L.; Huang, Z.L.; Zhou, J.X.; Guo, Q.J. The mixing of multi-source fluids in the Wusihe Zn–Pb ore deposit in Sichuan Province, Southwestern China. *Acta Geochim.* **2019**, *38*, 642–653. [[CrossRef](#)]

31. Xiong, S.F.; Gong, Y.J.; Jiang, S.Y.; Zhang, X.J.; Li, Q.; Zeng, G.P. Ore genesis of the Wusihe carbonate-hosted Zn–Pb deposit in the Dadu River valley district, Yangtze Block, SW China: Evidence from ore geology, S–Pb Isotopes, and sphalerite Rb–Sr Dating. *Miner. Depos.* **2018**, *53*, 967–979. [CrossRef]
32. Li, H.M.; Zhang, C.Q. The genetic relationship between the H₂S-bearing gas in Sichuan Basin and Lead-Zinc-Copper deposits around the basin. *Geol. Rev.* **2012**, *58*, 495–510. (In Chinese with English Abstract)
33. Luo, K.; Zhou, J.X.; Huang, Z.L.; Caulfield, J.; Zhao, J.X.; Feng, Y.X.; Ouyang, H.G. New insights into the evolution of Mississippi Valley-Type hydrothermal system: A case study of the Wusihe Pb–Zn deposit, South China, Using quartz in-Situ trace elements and sulfides in Situ S–Pb Isotopes. *Am. Mineral.* **2020**, *105*, 35–51. [CrossRef]
34. Wei, C.; Ye, L.; Li, Z.L.; Hu, Y.S.; Huang, Z.L.; Liu, Y.P.; Wang, H.Y. Metal sources and ore genesis of the Wusihe Pb–Zn deposit in Sichuan, China: New evidence from in-situ S and Pb Isotopes. *Acta Petrol. Sin.* **2020**, *36*, 3783–3796. (In Chinese with English Abstract) [CrossRef]
35. Tan, T.; Wang, G.Z.; Peng, H.L.; Huang, Z.; Zuo, L. Origin of ore-forming metal elements of MVT Pb–Zn deposit in Dengying formation, Sichuan Basin. *Mineral. Petrol.* **2021**, *41*, 68–79. (In Chinese with English Abstract) [CrossRef]
36. Hu, R.Z.; Fu, S.L.; Huang, Y.; Zhou, M.F.; Fu, S.H.; Zhao, C.H.; Wang, Y.J.; Bi, X.W.; Xiao, J.F. The giant South China Mesozoic low-temperature metallogenic domain: Reviews and a new geodynamic model. *J. Asian Earth Sci.* **2017**, *137*, 9–34. [CrossRef]
37. Zhao, X.F.; Zhou, M.F.; Li, J.W.; Sun, M.; Gao, J.F.; Sun, W.H.; Yang, J.H. Late paleoproterozoic to early Mesoproterozoic Dongchuan Group in Yunnan, SW China: Implications for tectonic evolution of the Yangtze Block. *Precambrian Res.* **2010**, *182*, 57–69. [CrossRef]
38. Zhu, L.M.; Yuan, H.H.; Luan, S.W. A study of isotopic geochemical features and mineralogical material source of the Disu and Daliangzi Pb–Zn deposits, Sichuan. *Mineral. Petrol.* **1995**, *15*, 72–79. (In Chinese with English Abstract) [CrossRef]
39. Zhang, C.Q.; Mao, J.W.; Wu, S.P.; Li, H.M.; Liu, F.; Guo, B.J.; Gao, D.R. Distribution, characteristics and genesis of Mississippi Valley -Type Lead-Zinc deposits in Sichuan-Yunnan-Guizhou area. *Miner. Depos.* **2005**, *24*, 336–348. (In Chinese with English Abstract) [CrossRef]
40. Li, H.M.; Chen, Y.C.; Wang, D.H.; Li, H.Q. Geochemistry and mineralization age of the Mayuan Zinc deposit, Nanzheng, Southern Shaanxi, China. *Geol. Bull. China* **2007**, *26*, 546–552. (In Chinese with English Abstract)
41. Liu, S.G.; Qin, C.; Jansa, L.; Sun, W.; Wang, G.Z.; Xu, G.S.; Yuan, H.F.; Zhang, C.J.; Zhang, Z.J.; Deng, B.; et al. Transformation of oil pools into gas pools as results of multiple tectonic events in Upper Sinian (Upper Neoproterozoic), deep part of Sichuan Basin, China. *Energy Explor. Exploit.* **2011**, *29*, 679–698. [CrossRef]
42. Yang, W.; Wei, G.Q.; Xie, W.R.; Jin, H.; Zeng, F.Y.; Su, N.; Sun, A.; Ma, S.Y.; Shen, J.H.; Wu, S.J. Hydrocarbon accumulation and exploration prospect of Mound-Shoal complexes on the platform margin of the fourth member of Sinian Dengying formation in the east of Mianzhu–Changning intracratonic rift, Sichuan Basin, SW China. *Pet. Explor. Dev.* **2020**, *47*, 1262–1274. [CrossRef]
43. Shi, C.H.; Cao, J.; Selby, D.; Tan, X.C.; Luo, B.; Hu, W.X. Hydrocarbon evolution of the over-mature Sinian Dengying reservoir of the Neoproterozoic Sichuan Basin, China: Insights from Re–Os geochronology. *Mar. Pet. Geol.* **2020**, *122*, 104726. [CrossRef]
44. Zheng, D.Y.; Pang, X.Q.; Luo, B.; Chen, D.X.; Pang, B.; Li, H.Y.; Yu, R.; Guo, F.X.; Li, W. Geochemical characteristics, genetic types, and source of natural gas in the Sinian Dengying formation, Sichuan Basin, China. *J. Pet. Sci. Eng.* **2021**, *199*, 108341. [CrossRef]
45. Wang, G.Z.; Liu, S.G.; Chen, C.H.; Wang, D.; Sun, W. The Genetic Relationship between MVT Pb–Zn Deposits and Paleo-Oil/Gas Reservoirs at Heba, Southeastern Sichuan Basin. *Earth Sci. Front.* **2013**, *20*, 107–116. Available online: https://www.researchgate.net/profile/Shugen-Liu/publication/285527458_The_genetic_relationship_between_MVT_Pb-Zn_deposits_and_paleo-oil-gas_reservoirs_at_Heba_Southeastern_Sichuan_Basin/links/597fc7280f7e9b8802ed2266/The-genetic-relationship-between-MVT-Pb-Zn-deposits-and-paleo-oil-gas-reservoirs-at-Heba-Southeastern-Sichuan-Basin.pdf (accessed on 13 October 2022). (In Chinese with English Abstract)
46. Gao, P.; Di Liu, G.; Lash, G.G.; Li, B.Y.; Yan, D.T.; Chen, C. Occurrences and origin of reservoir solid bitumen in Sinian Dengying formation dolomites of the Sichuan Basin, SW China. *Int. J. Coal Geol.* **2018**, *200*, 135–152. [CrossRef]
47. Liu, S.G.; Li, Z.Q.; Deng, B.; Sun, W.; Li, Z.W.; Ding, Y.; Song, J.M.; Wu, J. Occurrence morphology of bitumen in Dengying formation deep and Ultra-Deep carbonate reservoirs of the Sichuan Basin and Its indicating significance to oil and gas reservoirs. *Nat. Gas Ind.* **2021**, *41*, 102–112. (In Chinese with English Abstract) [CrossRef]
48. Wu, D.D.; Wu, N.Y.; Ye, Y.; Zhang, P.P.; Chen, X.G. Geochemical characteristics of hydrocarbon compounds in sediments of the Eastern South China Sea. *Acta Petrol. Sin.* **2008**, *29*, 517–526. (In Chinese with English Abstract) [CrossRef]
49. Moldowan, J.M.; Seifert, W.K.; Gallegos, E.J. Relationship between petroleum composition and depositional environment of petroleum source rocks. *Am. Assoc. Pet. Geol. Bull.* **1985**, *69*, 1255–1268. [CrossRef]
50. Blumer, M.; Guillard, R.R.L.; Chase, T. Hydrocarbons of marine phytoplankton. *Mar. Biol.* **1971**, *8*, 183–189. [CrossRef]
51. Mackenzie, F.T.; Bischoff, W.D.; Bishop, F.C.; Loijens, M.; Schoonmaker, J.; Wollast, R. Magnesian calcites; low-temperature occurrence, solubility and solid-solution behavior. *Rev. Mineral. Geochem.* **1983**, *11*, 97–144.
52. Huang, W. Geochemistry on Pyrobitumen and Source Rocks in Deep Layer of Leshan-Longnvisi Area. Master’s Thesis, China University of Petroleum, Beijing, China, 2017. (In Chinese with English Abstract)
53. Peters, K.E.; Moldowan, J.M. *The Biomarker Guide: Interpreting Molecular Fossils in Petroleum and Ancient Sediments*; Prentice Hall: Hoboken, NJ, USA, 1993; ISBN 0130867527.
54. Haven, H.L.T.; Leeuw, J.W.D.; Peakman, T.M.; Maxwell, J.R. Anomalies in steroid and hopanoid maturity indices. *Geochim. Cosmochim. Acta* **1986**, *50*, 853–855. [CrossRef]

55. Wolff, G.A.; Lamb, N.A.; Maxwell, J.R. The origin and fate of 4-methyl steroid hydrocarbons. I. diagenesis of 4-methyl sterenes. *Geochim. Cosmochim. Acta* **1986**, *50*, 335–342. [[CrossRef](#)]
56. Shen, C.B.; Ge, X.; Bai, X.J. Re-Os Geochronology Constraints on the Neoproterozoic-Cambrian Hydrocarbon Accumulation in the Sichuan Basin. *Earth Sci.* **2019**, *44*, 713–726. Available online: <http://www.earth-science.net/article/doi/10.3799/dqkx.2018.383> (accessed on 3 May 2022). (In Chinese with English Abstract)
57. Ge, X.; Shen, C.B.; Selby, D.; Wang, J.; Ma, L.B.; Ruan, X.Y.; Hu, S.Z.; Mei, L.F. Petroleum-generation timing and source in the Northern Longmen Shan Thrust belt, Southwest China: Implications for multiple oil-generation episodes and sources. *Am. Assoc. Pet. Geol. Bull.* **2018**, *102*, 913–938. [[CrossRef](#)]
58. Su, A.; Chen, H.H.; Feng, Y.X.; Zhao, J.X.; Wang, Z.C.; Hu, M.Y.; Jiang, H.; Nguyen, A.D. In situ U-Pb Dating and geochemical characterization of multi-stage dolomite cementation in the ediacaran Dengying formation, Central Sichuan Basin, China: Constraints on diagenetic, hydrothermal and Paleo-Oil filling events. *Precambrian Res.* **2022**, *368*, 106481. [[CrossRef](#)]
59. Wang, G.Z.; Liu, S.G.; Liu, W.; Fan, L.; Yuan, H.F. Process of hydrocarbon accumulation of Sinian Dengying formation in Gaoshiti structure, Central Sichuan, China. *J. Chengdu Univ. Technol. Technol. Ed.* **2014**, *41*, 684–693. (In Chinese with English Abstract) [[CrossRef](#)]
60. Su, A.; Chen, H.H.; Feng, Y.X.; Zhao, J.X.; Nguyen, A.D.; Wang, Z.C.; Long, X.P. Dating and characterizing primary gas accumulation in precambrian dolomite reservoirs, Central Sichuan Basin, China: Insights from pyrobitumen Re-Os and dolomite U-Pb geochronology. *Precambrian Res.* **2020**, *350*, 105897. [[CrossRef](#)]
61. Lin, Z.Y.; Wang, D.H.; Zhang, C.Q. Rb-Sr isotopic age of sphalerite from the Paoma Lead-Zinc deposit in Sichuan province and Its implications. *Geol. China* **2010**, *37*, 488–494. (In Chinese with English Abstract) [[CrossRef](#)]
62. Li, W.B.; Huang, Z.L.; Wang, Y.X.; Chen, J.; Han, R.S.; Xu, C.; Guan, T.; Yin, M.D. Age of the Giant Huize Zn–Pb Deposits Determined by Sm–Nd Dating of Hydrothermal Calcite. *Geol. Rev.* **2004**, *50*, 189–195. Available online: <http://www.corc.org.cn/handle/1471x/178531> (accessed on 16 September 2022). (In Chinese with English Abstract)
63. Zhang, Y.X.; Yue, W.; Guang, T.; Liang, S.; Zhou, Y.M.; Dong, W.W.; Rong, Z.; Yang, X.C.; Zhang, C.Q. Mineralization age and the source of ore-forming material at Lehong Pb–Zn deposit, Yunnan province: Constraints from Rb–Sr and S isotopes system. *Acta Mineral. Sin.* **2014**, *34*, 305–311. (In Chinese with English Abstract) [[CrossRef](#)]
64. Zhou, J.X.; Huang, Z.L.; Yan, Z.F. The origin of the Maozu carbonate-hosted Pb–Zn deposit, Southwest China: Constrained by C–O–S–Pb isotopic compositions and Sm–Nd isotopic age. *J. Asian Earth Sci.* **2013**, *73*, 39–47. [[CrossRef](#)]
65. Zhou, J.X.; Huang, Z.L.; Zhou, M.F.; Li, X.B.; Jin, Z.G. Constraints of C–O–S–Pb isotope compositions and Rb–Sr isotopic age on the origin of the Tianqiao carbonate-hosted Pb–Zn deposit, SW China. *Ore Geol. Rev.* **2013**, *53*, 77–92. [[CrossRef](#)]
66. Ohmoto, H.; Rye, R. Isotopes of sulfur and carbon. In *Geochemistry of Hydrothermal Ore Deposits*; John Wiley and Sons, Inc.: New York, NY, USA, 1979; pp. 505–567.
67. Chaussidon, M.; Lorand, J.P. Sulphur isotope composition of orogenic spinel lherzolite massifs from ariege (North-Eastern Pyrenees, France): An ion microprobe study. *Geochim. Cosmochim. Acta* **1990**, *54*, 2835–2846. [[CrossRef](#)]
68. Rollinson, H.R. *Using Geochemical Data: Evaluation, Presentation, Interpretation*; John Wiley and Sons: New York, NY, USA, 1993; ISBN 0582067014.
69. Claypool, G.E.; Holser, W.T.; Kaplan, I.R.; Sakai, H.; Zak, I. The age curves of sulfur and oxygen isotopes in marine sulfate and their mutual interpretation. *Chem. Geol.* **1980**, *28*, 199–260. [[CrossRef](#)]
70. Seal, R.R. Sulfur isotope geochemistry of sulfide minerals. *Rev. Mineral. Geochem.* **2006**, *61*, 633–677. [[CrossRef](#)]
71. Ohmoto, H.; Kaiser, C.J.; Geer, K.A. Systematics of sulphur isotopes in recent marine sediments and ancient sediment-hosted basemetal deposits. *Stable Isot. Stable Isot. Fluid Process. Miner.* **1992**, *23*, 70–120.
72. Machel, H. Bacterial and thermochemical sulfate reduction in diagenetic settings—Old and new insights. *Sediment. Geol.* **2001**, *140*, 143–175. [[CrossRef](#)]
73. Basuki, N.I.; Taylor, B.E.; Spooner, E.T.C. Sulfur isotope evidence for thermochemical reduction of dissolved sulfate in mississippi Valley-Type Zinc-Lead mineralization, Bongara Area, Northern Peru. *Econ. Geol.* **2008**, *103*, 783–799. [[CrossRef](#)]
74. Anderson, G.M. Kerogen as a source of sulfur in MVT deposits. *Econ. Geol.* **2015**, *110*, 837–840. [[CrossRef](#)]
75. Orr, W.L. Changes in sulfur content and isotopic ratios of sulfur during petroleum maturation—study of big horn basin paleozoic oils. *Am. Assoc. Pet. Geol. Bull.* **1974**, *58*, 2295–2318. [[CrossRef](#)]
76. Richardson, C.K.; Rye, R.O.; Wasserman, M.D. The chemical and thermal evolution of the fluids in the cave-in-rock fluorspar district, illinois; stable isotope systematics at the deardorff mine. *Econ. Geol.* **1988**, *83*, 765–783. [[CrossRef](#)]
77. Orr, W.L. Geologic and geochemical controls on the distribution of hydrogen sulfide in natural gas. *Geol. Soc. Am. Bull.* **1975**, *48*, 1220–1221.
78. Ohmoto, H.; Goldhaber, B. Sulphur and carbon isotopes. In *Geochemistry of Hydrothermal Ore Deposits*; John Wiley and Sons, Inc.: New York, NY, USA, 1997; pp. 517–600.
79. Thode, H.G.; Monster, J. Sulfur-isotope geochemistry of petroleum, evaporites, and ancient seas. *Fluids Subsurf. Environ.* **1965**, *24*, 21–27. [[CrossRef](#)]
80. Kiyosu, Y.; Krouse, H.R. The role of organic acid in the abiogenic reduction of sulfate and the sulfur isotope Effect. *Geochem. J.* **1990**, *24*, 21–27. [[CrossRef](#)]
81. MacGowan, D.B.; Surdam, R.C. Difunctional carboxylic acid anions in oilfield waters. *Org. Geochem.* **1988**, *12*, 245–259. [[CrossRef](#)]

82. Lu, J.L.; Yuan, Z.Q. Experimental Studies of Organic-Zn Complexes and Their Stability. *Geochimica* **1986**, *4*, 66–77. Available online: https://qikan.cqvip.com/Qikan/Article/Detail?id=8456886&from=Qikan_Article_Detail (accessed on 20 September 2022). (In Chinese with English Abstract)
83. Fu, J.M.; Peng, P.A.; Lin, Q.; Liu, D.H.; Jia, R.F.; Shi, J.X.; Lu, J.L. Several problems in the study of organic geochemistry of stratigraphic deposits. *Adv. Earth Sci.* **1990**, *5*, 43–49. (In Chinese)
84. Wang, G.Z.; Liu, S.G.; Su, W.C.; Sun, W.; Wang, D.; Yuan, H.F.; Xu, G.S.; Zou, C. Water Soluble Gas in Deep Carbonate Reservoir, Sichuan Basin, Southwest China. *J. Earth Ence* **2008**, *19*, 636–644. Available online: <http://en.earth-science.net/en/article/id/433> (accessed on 30 September 2022).